



Chromatin activity of I κ B α mediates the exit from naïve pluripotency

Reviewed Preprint

v1 • January 16, 2025

Not revised

Luis G Palma, Daniel Álvarez-Villanueva, María Maqueda, Mercedes Barrero, Arnau Iglesias, Joan Bertran, Damiana Álvarez-Errico, Carlos A García-Prieto, Cecilia Ballaré, Virginia Rodríguez-Cortez, Clara Bueno, August Vidal, Alberto Villanueva, Pablo Menéndez, Gregoire Stik, Luciano Di Croce, Bernhard Payer, Manel Esteller, Lluís Espinosa , Anna Bigas 

Program in Cancer Research. Hospital del Mar Research Institute, Barcelona, Spain • Josep Carreras Leukemia Research Institute, Barcelona, Spain • Centro de Investigación Biomédica en Red Cancer (CIBERONC), Madrid, Spain • Institut Investigació Biomèdica de Bellvitge (IDIBELL), L'Hospitalet de Llobregat, Barcelona, Spain • Centre for Genomic Regulation (CRG), The Barcelona Institute of Science and Technology, Barcelona, Spain • Faculty of Sciences, Technology and Engineering, Universitat de Vic - Universitat Central de Catalunya, Vic, Spain • Catalan Institute of Oncology (ICO/IDIBELL), L'Hospitalet de Llobregat, Barcelona, Spain • Spanish Network for Advanced Therapies (RICORS-TERAV). Carlos III Health Institute (ISCIII), Madrid, Spain • Department of Biomedicine. University of Barcelona, Barcelona, Spain • Institutio Catalana de Recerca i Estudis Avançats (ICREA), Barcelona, Spain • Universitat Pompeu Fabra, Barcelona, Spain • Physiological Sciences Department, School of Medicine and Health Sciences, University of Barcelona (UB), Barcelona, Spain

 https://en.wikipedia.org/wiki/Open_access

 Copyright information

eLife Assessment

This **important** study reveals a role for I κ B α in the regulation of embryonic stem cell pluripotency. The **solid** data in mouse embryonic stem cells include separation of function mutations in I κ B α to dissect its non-canonical role as a chromatin regulator and its canonical function as NF- κ B inhibitor. The conclusions could be strengthened by including better markers of differentiation status and additional controls or orthogonal approaches.

<https://doi.org/10.7554/eLife.102784.1.sa3>

Abstract

Summary

Maintenance of pluripotency is a multifactorial process in which NF- κ B is a negative regulator. Our previous work identified a chromatin role for I κ B α , the master regulator of NF- κ B signaling, that is critical for the proper regulation of various tissue stem cells. Here, we found that I κ B α accumulates specifically in the chromatin fraction of pluripotent embryonic stem cells. I κ B α depletion does not affect NF- κ B-dependent transcription, but causes a profound epigenetic rewiring in pluripotent stem cells, including alterations in H3K27me3, a histone mark catalyzed by Polycomb repression complex 2. Chromatin changes induced by I κ B α depletion affect a subset of pluripotency genes and are associated with altered gene transcription. At the cellular level, I κ B α -deficient embryonic stem cells are arrested in a naïve

pluripotency state when cultured in serum/LIF conditions and fail to exit pluripotency under differentiation conditions. By constructing separation-of-function mutants, we show that the effects of I κ B α in regulating stem cell pluripotency are NF- κ B-independent, but mainly rely on its chromatin-related function. Taken together, our results reveal a novel mechanism by which I κ B α participates in the regulation of the pluripotent state of embryonic stem cells and shed light on the interplay between inflammatory signals and the regulation of pluripotency.

Introduction

Embryonic Stem Cells (ESCs) pluripotency is characterized by the capacity to generate all somatic and germline lineages both *in vitro* and *in vivo*, depending on the culture conditions. When cultured in serum plus Leukemia Inhibitory Factor (LIF) (Serum/LIF), murine ESCs (mESCs) include cells interconverting to different metastable states¹ that either resemble preimplantation blastocyst (naïve pluripotency) or post-implantation (primed pluripotency) embryonic stages^{2–5}. The heterogeneity of mESCs in Serum/LIF is reduced by culturing them in the presence of GSK3 β and MEK1/2 inhibitors (CHIR99021 and PD0325901, respectively) along with LIF (2i/LIF). Under these conditions, mESCs enter a ground state of naïve pluripotency characterized by self-renewal activity while suppressing any pro-differentiating signals^{6,7}. This pluripotent state closely resembles the inner cell mass of the E4.0 mouse preimplantation blastocyst⁸. After implantation, pluripotent capability of the mouse embryo (E5.5) becomes restricted to Epiblast Stem Cells (EpiSCs), which represent a primed pluripotent state, characterized by coexpression of pluripotency and lineage specification markers^{9,10}. EpiSCs can give rise to cells from the three germ layers (endoderm, mesoderm and ectoderm), albeit their contribution to chimeras or to germ cells is greatly compromised^{4,11}. EpiSCs can be derived *in vitro* from naïve pluripotent cells when cultured in a medium supplemented with Nodal and fibroblast growth factor (FGF)¹². Different epigenetic features distinguish naïve from primed pluripotent states¹³, such as changes in the X chromosome inactivation in female cells^{12,14}, histone post-translational modifications¹⁰ or a global DNA hypomethylation profile observed in naïve pluripotent stem cells^{15–17}. These epigenetic changes are a prerequisite for the subsequent activation of gene circuits associated with pluripotency exit and germ layer specification^{9,10}. Crucial regulatory elements for the transition from naïve to primed pluripotency state are located in distal DNA regions or enhancers to facilitate the resolution toward the primed state^{18,19}. Therefore, identifying novel players to fine-tune the equilibrium between ground and primed states is crucial for preserving both pluripotency stability and differentiation capability in mESCs.

There is now strong evidence that inflammatory signals are critical for stem cell development^{20–22}, with NF- κ B being the main effector. Different strategies to inhibit or attenuate NF- κ B in ESCs lead to increase pluripotency gene expression and impair cell differentiation^{23,24}, or it facilitates reprogramming to induced pluripotent stem cells (iPSC)²⁵. Canonical NF- κ B signaling is triggered by the IKK kinase complex, which induce the phosphorylation and subsequent degradation of the NF- κ B inhibitor, I κ B α , leading to nuclear translocation of the NF- κ B factors (e.g. p50/p65)²⁶. However, we have previously identified a nuclear I κ B α function, which is critical for tissue stem cell homeostasis and the proper differentiation of epidermal, intestinal and hematopoietic stem cells^{27–30}. I κ B α chromatin function is mediated by the interaction with histone deacetylases (HDACs), core elements of the Polycomb Repressor Complex 2 (PRC2) and histone H2A and H4^{27,29,31}.

We have now investigated the role of I κ B α in the context of pluripotent stem cells. Whereas cytoplasmic I κ B α is detected in the different states and its levels decrease after differentiation, in agreement with NF- κ B activity as a promoter of differentiation, we specifically detected chromatin-bound I κ B α in the naïve pluripotent stem cells. Importantly, I κ B α depletion in ESCs did not affect NF- κ B activity but it stabilizes the naïve (2i/LIF-like) state of pluripotency under

Serum/LIF conditions, displaying an epigenetic rewiring, including changes in the PRC2-dependent H3K27me3 histone mark and impacting in proximal and distal regulation of pluripotent genes. Using a new Separation-Of-Function (SOF) IκBα mutants³², we have now definitively demonstrated that chromatin-bound IκBα is required for naïve pluripotency exit of mESCs in an NF-κB-independent manner. Overall, we identified IκBα as a novel key player in the regulation of the exit from naïve-to-primed pluripotency and essential for the activation of gene programs involved in germ layer specification.

Results

IκBα and NF-κB have opposite expression dynamics in naïve pluripotent cells

Due to the prominent role of NF-κB signaling in mESCs regulation, we analyzed the expression pattern of the different NF-κB members including the IκB inhibitors in the three defined pluripotent stages: ground state of naïve pluripotency (2i/LIF), naïve pluripotency (Serum/LIF), and primed pluripotency (Epiblast Stem Cells or EpiSCs)⁵ (**Figure 1A**). In agreement with NF-κB being a pro-differentiation factor, canonical NF-κB inhibitors including IκBα (*Nfkb1*), IκBβ (*Nfkb2*) and IκBε (*Nfkb3*) were all expressed in the naïve pluripotency state (both 2i/LIF and Serum/LIF), with *Nfkb1* levels gradually reduced upon naïve pluripotency exit towards EpiSCs (**Figure 1B**). In contrast, *Rela*, *Nfkb1* and *Nfkb2* genes, codifying for the NF-κB factors p65/RelA, p105 and p100, respectively, showed opposite expression dynamics increasing the levels in EpiSCs (**Figure 1C**). We further characterized the distribution of IκBα in the cytoplasm, nucleus and chromatin fractions of the three states of pluripotency (**Figure 1D**). Total IκBα protein levels correlated with the detected RNA levels in the three different cellular states being highest in the 2i/LIF condition (**Figure 1B**), with a large accumulation in the cytoplasm. A fraction of IκBα protein was detected in the chromatin of naïve pluripotent cells, being highest in cells cultured in Serum/LIF conditions compared to 2i/LIF and absent in the EpiSCs. (**Figure 1D**). The dynamics of IκBα RNA and protein levels from naïve pluripotent ESCs to EpiSCs was further corroborated by analysis of an additional database that includes both naïve and primed pluripotent states³³ (**Figure 1E**).

Next, we studied IκBα expression in differentiated embryoid bodies (EBs) from mESCs (Serum/LIF) (see materials and methods) and analyzed the expression levels of different pluripotency, differentiation-linked, and NF-κB genes by RNA sequencing. *Nfkb1* (IκBα gene) was expressed at higher levels specifically in mESCs (Serum/LIF) whereas cells undergoing differentiation (48h and 96h) displayed a reduction in its expression levels (**Figure 1F**). The expression pattern of *Nfkb1* was similar to the pluripotency genes whereas most of the NF-κB genes were upregulated upon differentiation, clustering together with developmental genes, as previously described²⁴. Notably, several polycomb elements were highly expressed in mESCs, consistent with the possibility that chromatin-bound IκBα modulates PRC2 activity²⁷ in the pluripotent state.

Taken together, these data show that, unlike the other NF-κB inhibitors and target genes, the expression of *Nfkb1* is high in the naïve pluripotent state, with IκBα protein present in the cytoplasm and chromatin of naïve pluripotent cells. Moreover, whereas canonical NF-κB subunits are primarily absent, we detected several Polycomb elements expressed in mESCs.

IκBα is required in mESCs to exit the naïve pluripotency state

To investigate the functional implication of IκBα in naïve pluripotency, we knocked-out (KO) IκBα protein in mESCs by CRISPR-Cas9 (IκBα-KO mESCs) (**Figure S1A** and materials and methods). Notably, IκBα KO mESCs have an impaired ability to undergo differentiation and cannot properly switch off the pluripotency program after 216h (9 days) of pro-differentiation signals, as it is

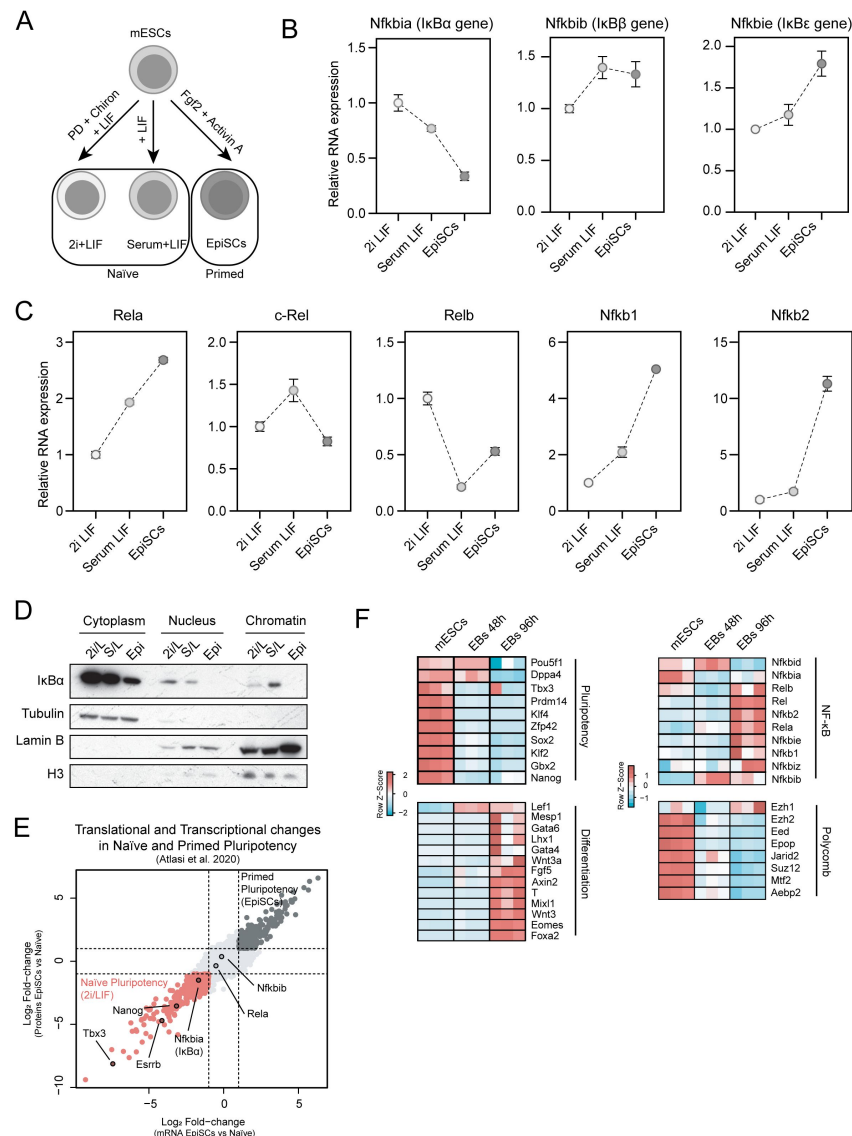


Figure 1.

I κ B α is highly expressed in pluripotent cells.

A. Schematic of pluripotent states in mouse embryonic stem cells (mESCs). mESCs were maintained regularly in naïve pluripotency by culturing them in serum/LIF medium, or they were polarized towards the ground state of naïve pluripotency by culturing them for two passages in LIF plus Gsk3 β (CHIR99021 or Chiron) and MEK (PD0325091) inhibitors (2i/LIF). mESCs were further differentiated towards the primed pluripotent state (epiblast-like cells) by culturing mESCs in a medium containing 20ng/mL Activin A and 10ng/mL Fgf2 for 120h. **B-C.** Relative mRNA levels (based on qPCR experiments) of the canonical I κ B genes (*Nfkbia*, *Nfkbib*, *Nfkbie*) or NF- κ B effector genes (*Rela*, *c-Rel*, *Relb*, *Nfkb1*, *Nfkb2*) across the different states of pluripotency. Expression was normalized using the house-keeping gene *Tbp* relative to 2i/LIF. Data from three independent experiments. Dots indicate mean values and error bars refer to \pm standard deviation (SD). **D.** Western blot analysis of I κ B α protein distribution in cytoplasm, nucleoplasm (Nucleus) or chromatin in cells at the ground-state of naïve pluripotency (2i/L), naïve pluripotency (S/L) or primed pluripotency (Epi). **E.** Transcriptome and proteome differences across naïve (2i/LIF) and primed (Epiblast-like cells or EpiSCs) pluripotent states. Enriched transcripts and proteins in naïve state are highlighted in red (Log2 fold-change < -1). Enriched transcripts and proteins in the primed state are marked in dark gray (Log2 fold-change > 1). Data from 33. **F.** Heatmap showing the expression levels of pluripotency (*Dppa4*, *Pou5f1*, *Sox2*, *Prdm14*, *Klf4*, *Zfp42*, *Nanog*), differentiation (*Mesp1*, *Gata6*, *Gata4*, *Lhx1*, *Wnt3a*, *Fgf5*, *Nes*, *Axin2*, *Wnt3*, *Eomes*, *Foxa2*, *T*, *Mixl1*, *Lef1*) NF- κ B (*Nfkbia*, *Nfkbib*, *Nfkbie*, *Nfkbiz*, *Rela*, *c-Rel*, *Relb*) and Polycomb (*Ezh1*, *Ezh2*, *Eed*, *Epop*, *Jarid2*, *Suz12*, *Mtf2*, *Aebp2*) genes from the RNAseq samples at mESCs (Serum/LIF) and differentiating cells (embryoid bodies) at 48h and 96h of I κ B α -WT cells. Normalized counts based on z-score are represented.

demonstrated by high levels of pluripotency markers OCT3/4 and NANOG (Fig 1A and Fig S1C), higher number of alkaline phosphatase cells (Fig 1B and Fig S1) and higher percentage of SSEA-1⁺ cells (Fig S1B) within the 216h EBs. These results were also supported by the detection of increased expression level of the naïve pluripotency genes *Pou5f1* (*Oct3/4* gene), *Gbx2*, *Klf2*, *Sox2*, *Zfp42* (*Rex1*) and *Nanog* in IκBα KO EBs after 216h of differentiation (Figure S1B).

To shed light into the molecular mechanisms governing the differentiation impairment in IκBα KO EBs, we performed RNA-seq of IκBα WT and IκBα KO mESCs in the first stages of the embryoid body differentiation. Analysis of the data indicated that IκBα KO EBs cannot successfully evolve towards differentiation trajectories, as shown by principal component analysis (PCA) of IκBα-WT and IκBα-KO EBs at 48h and 96h in differentiation media (Figure 2C). Analysis of naïve pluripotency markers at 96h (*Gab1*, *Sox2*, *Esrrb*, *Zfp42*, *Dppa4*, *Klf2*, *Prdm14*, *Klf4*, *Tfcp2l1*) also showed higher expression levels in IκBα KO compared to their IκBα WT counterparts (Figures 2D and S1F). Defective differentiation capacity of IκBα KO EBs involved programs associated with specification of all 3 germ layers (endoderm, mesoderm, and ectoderm) (Figures 2E-G). Moreover, IκBα KO EBs were smaller in size (Figure S1E), in agreement with the reduced developmental potential of IκBα-depleted mESCs³⁴. To further study the requirement of IκBα in pluripotency exit *in vivo*, we established teratomas by subcutaneous injection of IκBα-WT and IκBα-KO mESCs (Figure 2H and materials and methods) into NSG (NOD.Cg-Prkdc^{cid} Il2rg^{tm1Wjl}/SzJ) mice. IκBα-KO teratomas showed a decreased differentiation potential, as indicated by higher number of OCT4⁺ cells 6 weeks after injection (Figures 2H-J). These observations further confirm the essential role of IκBα in the exit from the pluripotency state not only *in vitro* but also under *in vivo* differentiation signals. To understand the conditions in which IκBα is required for pluripotency exit, we differentiated IκBα-WT and IκBα-KO mESCs cultured in Serum/LIF (naïve pluripotency) towards EpiSCs (primed pluripotency) (Figure 3A, upper panel). IκBα-KO cells were not committed towards the primed pluripotency stage and maintained an elevated expression levels of naïve pluripotency genes (*Dppa3*, *Nanog*, *Sox2*, *Rex1*, *Klf2*, *Klf4*, *Gbx2*, *Tbx3*) (Figure 3A, bottom panel). Additionally, IκBα-KO cells retained a naïve pluripotent morphology, forming tight clusters that resemble cells cultured in 2i/LIF medium (Figure S2A).

mESCs cultured in serum/LIF are highly heterogeneous, comprising a mixture of cell states that resemble developmental transitions from preimplantation (naïve pluripotency) to postimplantation (primed pluripotency) embryo^{2,3}. To investigate how IκBα deficiency was affecting the exit of mESCs from naïve pluripotency, we performed a Gene Set Enrichment Analysis (GSEA) using RNA-seq data from IκBα-KO and IκBα-WT mESCs cultured in Serum/LIF against gene signatures for 2i/LIF and Serum/LIF pluripotency³⁵. GSEA results revealed a significant enrichment in Serum/LIF IκBα-KO mESCs transcriptome for genes specifically expressed in the naïve ground state (2i/LIF), while they negatively correlate with mESCs cultured in Serum/LIF (Figure 3B)³⁵. These results agree with the fact that IκBα-KO mESCs cultured in Serum/LIF resemble 2i/LIF morphology, with homogeneous tight clusters of cells, whereas IκBα-WT mESCs retain the colony heterogeneity (Figure S2B). Interestingly, the higher levels of ground-state-related genes *Zfp42* (*Rex1*), *Klf2* and *Tbx3* in IκBα-KO mESCs were partially obtained when IκBα-WT mESCs were cultured in 2i/LIF for two consecutive passages (Figure 3C).

One of the key features of the naïve pluripotency state is its global DNA hypomethylation pattern^{15,16}. We assessed the DNA methylation status of IκBα-WT and IκBα-KO mESCs cultured in Serum/LIF conditions by analysis of 5-methyl-cytosine (5mC) mark and using DNA methylation arrays³⁶. We found that IκBα-KO mESCs contained much lower levels of 5mC compared to IκBα-WT cells (Figure 3D). Moreover, DNA methylation arrays confirmed a global pattern of DNA hypomethylation in IκBα-KO mESCs, which was maintained in 96h EBs (Figure 3E). Interestingly, the DNA hypomethylation status occurred in a genome-wide fashion affecting all chromosomes (Figure S2C), in accordance with a higher pluripotent state of IκBα-KO mESCs.

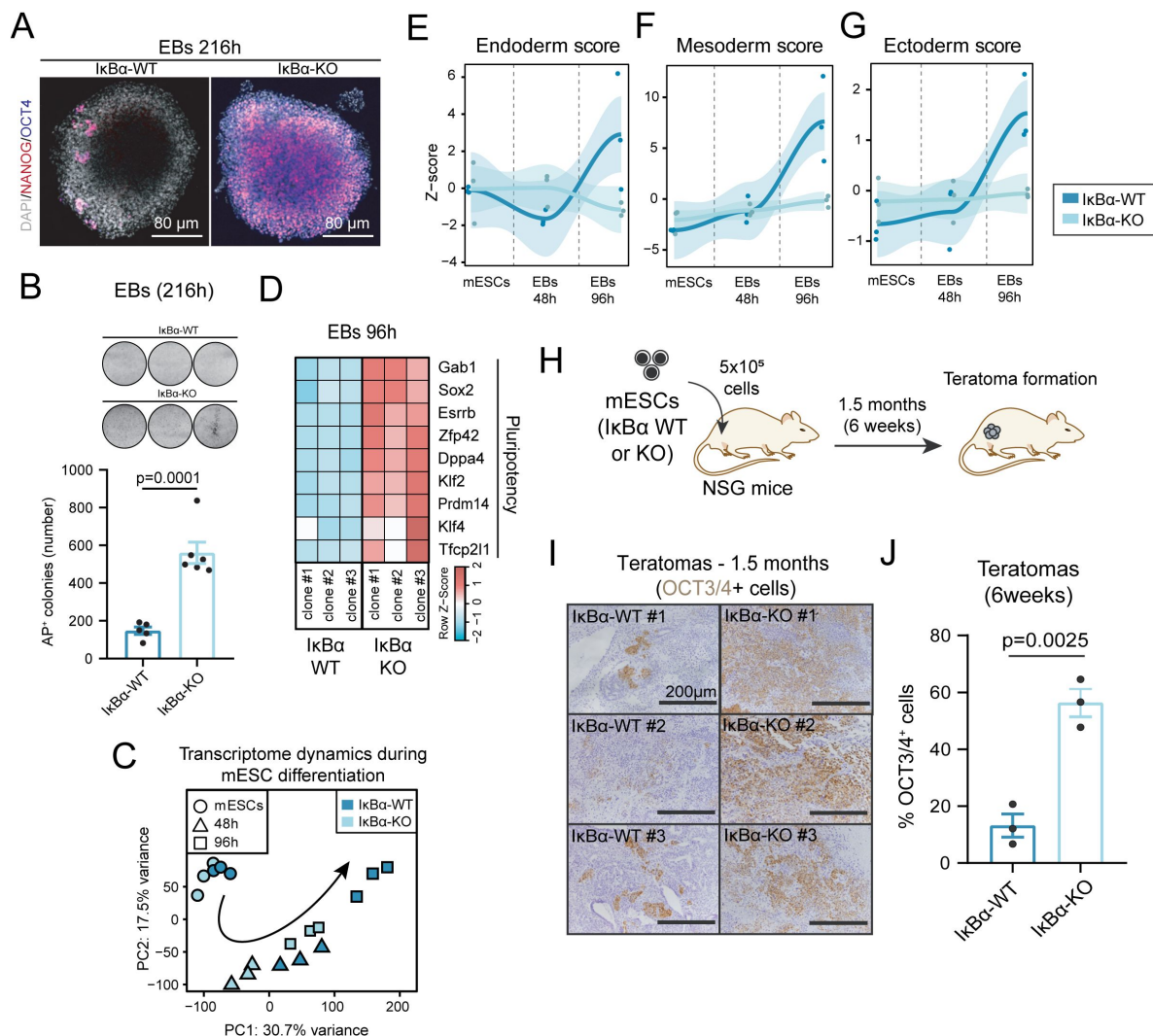


Figure 2.

The absence of IκBα hinders the exit from the pluripotent state and prevents the activation of differentiation programs.

A. Representative immunofluorescence of 216h EBs stained with the pluripotency markers NANOG and OCT3/4. **B.** Quantification of total number of alkaline phosphatase (AP) colonies after 216h EB differentiation and additional culture of 96h in Serum/LIF (S/L) medium. Dots represent values from two independent experiments from three different IκBα-WT or IκBα-KO clones. Unpaired two-sided t-test applied. Representative images from AP colonies are included in the upper panel. **C.** PC1 and PC2 from Principal Component Analysis (PCA) of normalized RNA-seq data from 3 different time points (mESCs, 48h EBs and 96h EBs) of IκBα-WT and IκBα-KO cells (three independent clones from each genotype). **D.** Heatmap showing the expression levels of naïve pluripotency genes (*Gab1*, *Sox2*, *Esrrb*, *Zfp42*, *Dppa4*, *Klf2*, *Prdm14*, *Klf4*, *Tfcp2l1*) from the RNAseq samples of IκBα-WT and IκBα-KO EBs at 96h. Normalized counts based on z-score are represented. **E-G.** Z-score values for gene sets referring to Endoderm (E), Mesoderm (F) and Ectoderm (G) formation from The Gene Ontology database (GO:0001706, GO:0001707 and GO:0001705 terms, respectively) and obtained from corresponding expression levels at mESCs, 48h and 96h EBs IκBα-WT or IκBα-KO cells (three independent clones of each genotype). Loess curves are also represented with 95% confidence intervals (shadowed area surrounding the curves). **H.** Schematic of teratoma formation assay. 5x10⁵ IκBα-WT or IκBα-KO mESCs cultured in Serum/LIF were injected intramuscularly in the leg of immunocompromised NSG mice. 6 weeks after the transplant, teratomas were formed, and mice were euthanized for further teratoma analysis. **I.** Representative images of immunohistochemistry for OCT3/4 in IκBα-WT (left panel) or IκBα-KO (right panel) teratomas. Teratomas were derived from three independent clones of mESCs of both genotypes. **J.** Percentage of OCT3/4⁺ cells in teratomas. Positive cells were counted from five different microscope fields from each IκBα-WT and IκBα-KO clone. Unpaired two-sided t-test was performed. Bars indicate mean values and error bars refer to ± SD.

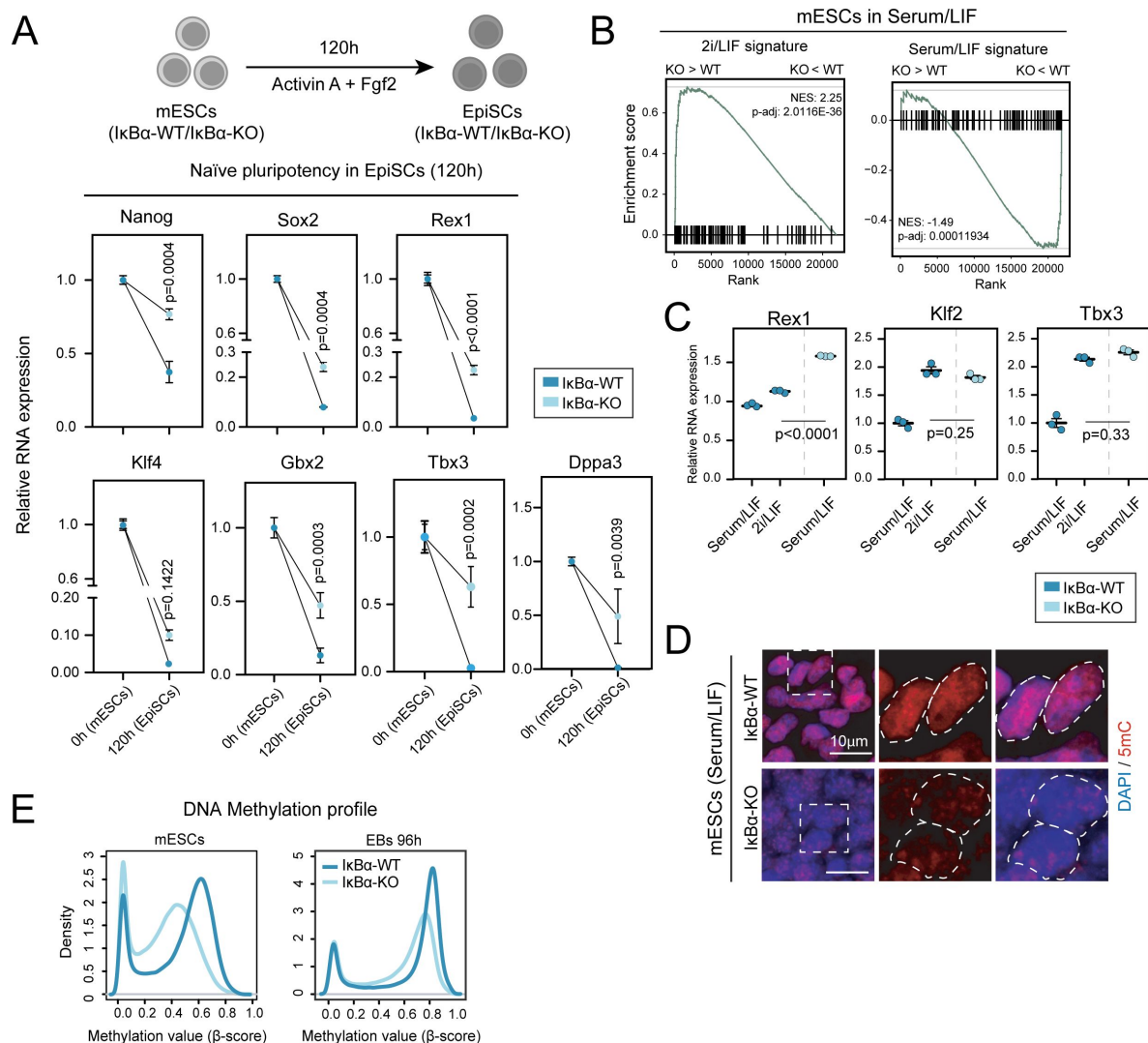


Figure 3.

IkBa-KO mESCs retain the ground-state of naïve pluripotency under Serum/LIF culture.

A. (Upper panel) Schematics of mESCs differentiation towards Epiblast Stem Cells (EpiSCs). mESCs cultured in Serum/LIF were then seeded in N2B27 medium supplemented with 10ng/mL Fgf2 and 20ng/mL Activin A for 120h (see Materials and Methods section for further information). (Bottom panel) Relative RNA levels (based on qPCR experiments) of naïve pluripotency genes (*Nanog*, *Sox2*, *Rex1*, *Klf4*, *Gbx2*, *Tbx3*, *Dppa3*) in IkBa-WT or IkBa-KO EpiSCs at 120h. RNA levels were normalized based on *Tbp* expression relative to IkBa-WT. Each dot represents an independent clone either from IkBa-WT or IkBa-KO genotypes. Unpaired two-sided t-test applied. Horizontal bars indicate mean values and error bars refer to \pm SD. **B.** GSEA results comparing IkBa-KO vs IkBa-WT mESCs cultured in Serum/LIF against ground (2i/LIF) and naïve (Serum/LIF) state pluripotency signatures retrieved from [35](#). Adjusted p-value by Benjamini-Hochberg procedure and Normalized Enrichment Score (NES) indicated. **C.** Relative RNA levels of the naïve pluripotency genes *Rex1* (*Zfp42*), *Klf2* and *Tbx3* upon culture of IkBa-WT either in Serum/LIF or two passages in 2i/LIF. 2i/LIF IkBa-WT mESCs were compared with IkBa-KO mESCs cultured in Serum/LIF. Unpaired two-sided t-test was applied to calculate statistical significance. Each dot represents an independent clone from each of the two genotypes. **D.** Representative immunofluorescence images of DNA-methylation-related mark 5-methylcytosine (5mC) in IkBa-WT (left) and IkBa-KO (right) mESCs cultured in Serum/LIF. **E.** DNA methylation profile (using DNA methylation arrays [36](#)) in IkBa-WT vs IkBa-KO mESCs (upper) and 96h EBs (bottom panel) showing the distribution density of mean β -values from all 261,220 CpGs under test per condition.

Overall, these data demonstrate that I κ B α is required for the exit of the naïve state of pluripotency and its deficiency results in impaired differentiation of mESCs *in vivo* and *in vitro*. Accordingly, I κ B α -KO mESCs cultured in Serum/LIF showed genome-wide pattern of DNA hypomethylation.

Lack of I κ B α causes an epigenetic rewiring in pluripotent stem cells to resemble 2i/LIF naïve pluripotency in Serum/LIF culture

ChIP Enrichment Analysis (ChEA) of genes identified in our RNA-seq data of I κ B α -KO and WT mESCs revealed that differentially expressed genes were putative targets of chromatin regulators including the PRC2 subunit SUZ12 and MTF2 (Figure 4A). We previously described that I κ B α is important for the proper deposition of the H3K27me₃ mark in different types of tissue stem cells by associating with elements of the PRC2 complex^{27,28}. Since 2i/LIF and Serum/LIF states are characterized by important differences in epigenetic marks, we carried out an epigenetic profiling of I κ B α -WT and I κ B α -KO mESCs cultured in Serum/LIF. We performed chromatin immunoprecipitation followed by sequencing (ChIP-seq) of histone modifications associated with gene activation (H3K4me₃) and gene repression (H3K27me₃) (Figures 4B and S3A-B). Overall, Serum/LIF I κ B α -KO mESCs exhibited a general increased H3K4me₃ status and redistribution of the PRC2-catalyzed H3K27me₃ mark (Figure 4B). Notably, gain of the H3K4me₃ mark was associated with a reduction of H3K27me₃ levels in genes associated with naïve pluripotency function (Figures 4B-C and S3A-B). In particular, 41 genes with concomitant gain of H3K4me₃ and loss of H3K27me₃ were found to be enriched in mechanisms associated with pluripotency function (Figure 4C), including Tbx3 and Gbx2 (Figure 4D-E). A second set of pluripotency-related genes showed an increase in H3K4me₃ without changes in H3K27me₃ (Zfp42 or Klf2). Both sets of pluripotency genes showed increased expression in the absence of I κ B α (Figure 4H).

We next aimed to study whether the lack of I κ B α was also affecting distal regulatory regions by analyzing enhancer-associated histone marks in I κ B α -WT and I κ B α -KO mESCs. We quantified the total amount of H3K27Ac (active enhancer) and H3K4me₁ (poised enhancer) by ChIP-seq experiments conducted in both I κ B α -WT and I κ B α -KO mESCs. Overall, I κ B α -KO mESCs showed a reduction in poised enhancers at genes (or related genomic regions) associated with differentiation processes (Figures 4F and S3C) and an increase in active enhancers at genes associated with pluripotency (Figure 4F and S3D), such as Tbx3, Tfcp2l1 and Zfp42 (Rex1) (Figure 4G), which positively favors their higher expression in I κ B α -KO mESCs (Figure 4H). These results further support that mESCs lacking I κ B α are epigenetically remodeled to favor the ground state of naïve pluripotency, which may negatively impact on their differentiation potential, similar to that described for other models with stabilized naïve pluripotent state^{37,38}.

The chromatin function of I κ B α in pluripotency exit is independent of classical NF- κ B activity

Although previous results from *C. elegans*³⁹ and *Drosophila*²⁷ support the functional relevance of chromatin-related I κ B α function, the investigation of this alternative I κ B α activity remains challenging due to the predominant role of this protein in NF- κ B regulation. However, and similar to that found in other models, we did not detect major changes in canonical NF- κ B target genes upon I κ B α depletion neither in Serum/LIF mESCs, nor 48h and 96h EB-differentiating conditions (Figure 5A). Thus, either NF- κ B regulation does not require I κ B α at this stage or it might be compensated by the other I κ Bs (I κ B β , I κ B ϵ or p100), as previously demonstrated^{40,41}. This observation suggests that either NF- κ B signaling is not active in naïve pluripotency, which is supported by the low expression levels of NF- κ B subunits (see Figures 1B-C and 1E-F), or I κ B α function on NF- κ B is compensated by the other I κ Bs (I κ B β , I κ B ϵ or p100), as previously demonstrated^{40,41}.

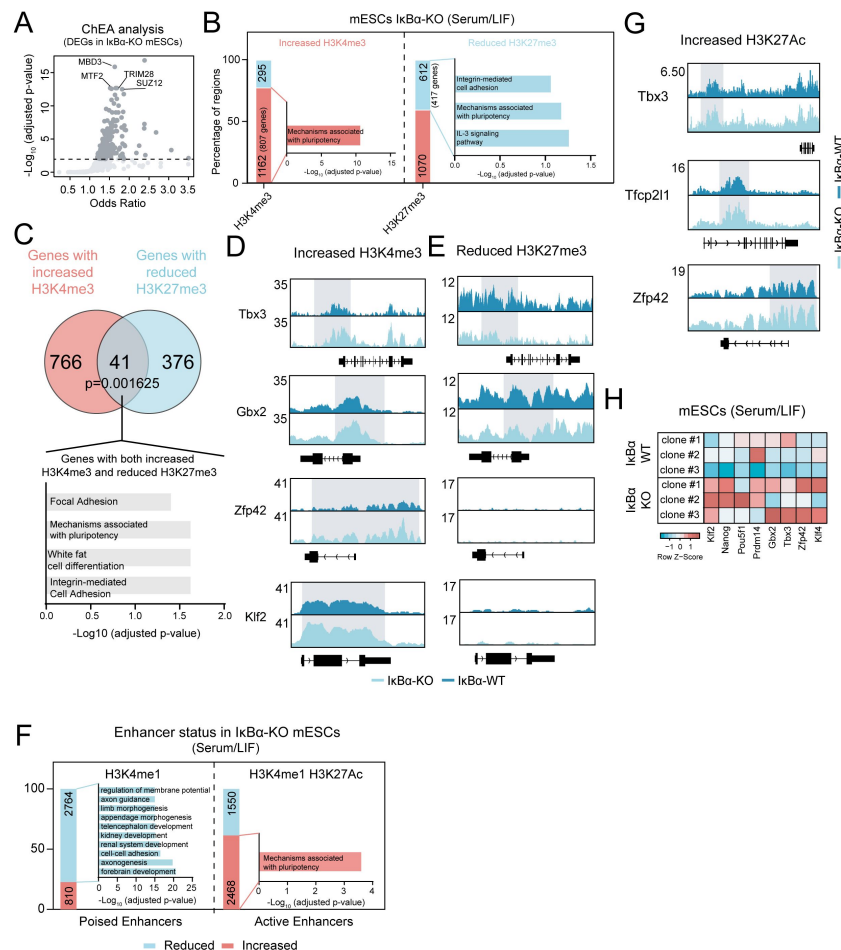


Figure 4.

Absence of IκBα reinforces the pluripotency program at the epigenetic and transcriptional levels.

A. ChIP-seq Enrichment Analysis (ChEA) of differentially expressed genes (DEGs; adjusted p-value<0.05) in IκBα-KO mESCs. P-value was calculated using Fisher exact test. **B.** Number of differentially bound regions (adjusted p-value <0.05, FDR) for H3K4me3 and H3K27me3 histone marks in IκBα^{-/-} vs IκBα^{+/+} mESCs cultured in Serum/LIF. Enriched or reduced regions in IκBα^{-/-} mESCs are distinguished (log2 Fold-change >0 or <0, respectively). Overrepresented WikiPathways, for (left) H3K4me3 and (right) H3K27me3 are indicated. Annotated genes to differential regions showing H3K4me3 enrichment or H3K27me3 reduction were considered. A one-sided hypergeometric test was conducted. **C.** Venn Diagram of genes contained in regions with either increased H3K4me3 or reduced levels of H3K27me3. Statistical significance of the overlapping was calculated using the chi-squared method. Overrepresented pathways for genes containing increased H3K4me3 and reduced H3K27me3 levels are indicated (only pathways with an adjusted p-value<0.05 were considered). **D-E.** Representative genomic regions of naïve pluripotency genes having either differential enriched H3K4me3-only (D) or reduced H3K27me3-only (E) levels in IκBα-KO vs IκBα-WT mESCs cultured in Serum/LIF. Shadowed regions highlight the differential levels of the histone marks. **F.** Number of regions with differential enhancer activity in IκBα-KO vs IκBα-WT mESCs cultured in Serum/LIF. Increased/Reduced activity for (left) poised enhancers based on the H3K4me1 differential binding and absence of H3K27ac overlapping peaks in IκBα-KO mESCs and, (right) active enhancers based on the differential binding of H3K27ac and presence of H3K4me1 overlapping peaks in IκBα-KO. Differential binding based on adjusted p-value <0.05 (FDR). Increased or reduced regions in IκBα-KO are distinguished by log2 Fold-change >0 or <0, respectively, compared to IκBα-WT mESCs. Overrepresented WikiPathways for annotated genes to (left) poised enhancers with reduced activity and (right) active enhancers with increased activity in IκBα-KO vs IκBα-WT mESCs are indicated (adjusted p-value < 0.05, FDR). A one-sided hypergeometric test was conducted. **G.** Representative genomic regions of naïve pluripotency genes having an increase in active enhancer status (H3K27Ac enrichment) in IκBα-KO mESCs cultured in Serum/LIF. Shadowed regions highlight the differential levels of the histone mark. **H.** Heatmap showing the expression levels of the naïve pluripotency genes from the RNAseq samples of IκBα-KO and IκBα-WT mESCs cultured in Serum/LIF. Normalized counts (z-score) from genes are represented.

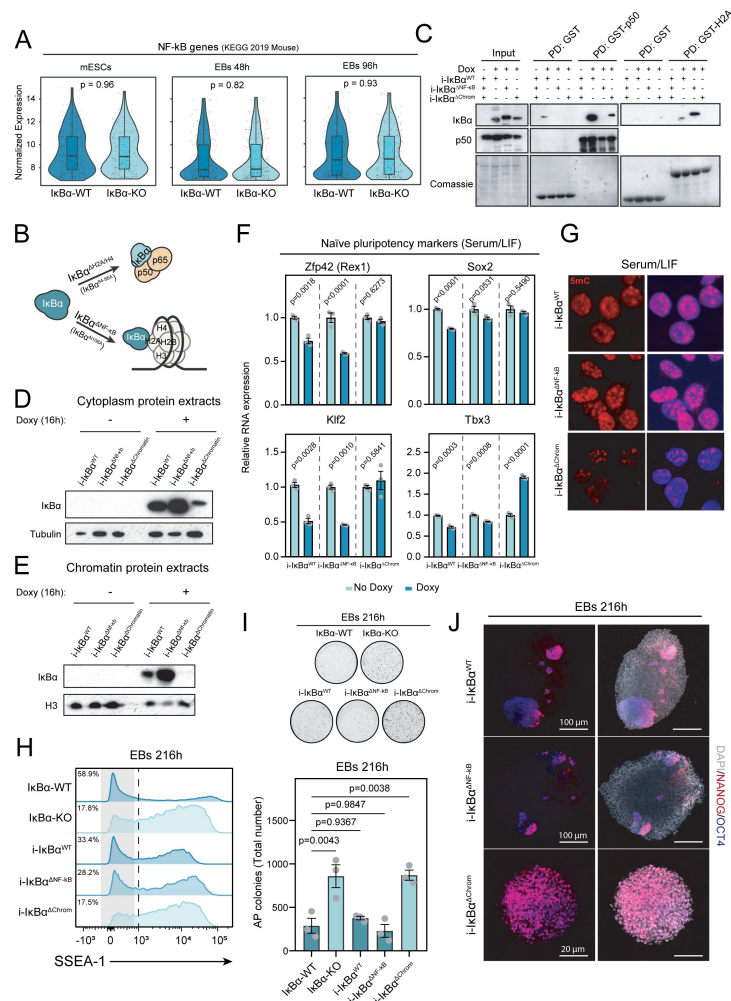


Figure 5.

IκBα prevents the hyperactivation of naïve pluripotency program in an NF-κB-independent manner.

A. Boxplots, violin plots and individual values representing the normalized gene expression levels in IκBα-WT or IκBα-KO mESCs, EBs 48h and EBs 96h. Considered genes are those annotated to NF-κB signaling pathway (KEGG PATHWAY mmu04064). Box Plots: center line, median; lower and upper hinges, first and third quartiles; whiskers, 1.5x interquartile range (IQR) extended to the largest/smallest value within 1.5xIQR; no outliers present. Unpaired two-sided Wilcoxon test applied. **B.** Schematic of chromatin-specific/NF-κB-deficient (IκBα^{ΔNF-κB}) or NF-κB-specific/chromatin-deficient (IκBα^{ΔChrom}) IκBα mutants (Separation-Of-Function or SOF mutants). **C.** Pull-down of GST-H2A and GST-P50 with cell lysates from different SOF IκBα mutant mESCs. **D.** Western blot analysis of cytoplasmic protein extracts of doxycycline-inducible IκBα forms (i-IκBα^{ΔWT}, i-IκBα^{ΔNF-κB}, i-IκBα^{ΔChrom}) after 16h of doxycycline induction. **E.** Western blot analysis of chromatin protein extracts of doxycycline-inducible IκBα forms (i-IκBα^{ΔWT}, i-IκBα^{ΔNF-κB}, i-IκBα^{ΔChrom}) after 16h of doxycycline induction. **F.** Relative RNA levels of naïve pluripotency genes (*Zfp42*, *Klf2*, *Sox2*, *Tbx3*) in i-IκBα^{WT}, i-IκBα^{ΔNF-κB} and i-IκBα^{ΔChrom} mESCs after doxycycline induction. Unpaired two-sided t-test was performed. Bars indicate mean values and error bars refer to ± SEM. **G.** Representative immunofluorescence images of DNA-methylation-related mark 5-methylcytosine (5mC) in i-IκBα^{WT} (upper panel), i-IκBα^{ΔNF-κB} (medium panel), i-IκBα^{ΔChrom} (bottom panel) mESCs cultured in Serum/LIF. **H.** Flow cytometry analysis of the pluripotency surface marker SSEA-1 at 216h EBs in i-IκBα^{WT}, i-IκBα^{ΔNF-κB} and i-IκBα^{ΔChrom} cells. **I.** Quantification of Alkaline Phosphatase (AP) staining in 216h EBs upon reconstitution with the different IκBα forms. Each dot represents an independent experiment. One-way ANOVA was applied. Bars indicate mean values and error bars refer to ± SEM. Representative images of Alkaline Phosphatase (AP) staining in 216h EBs are included in the upper panel. **J.** Representative immunofluorescence for NANOG and OCT3/4 at 216h EBs in i-IκBα^{WT} (upper panel), i-IκBα^{ΔNF-κB} (medium panel) and i-IκBα^{ΔChrom} (bottom panel) cells.

To further investigate the relative impact of both IκBα functions in mESCs, we took advantage of recent results from our group that led to the identification of the specific IκBα protein residues that define NF-κB- or chromatin-binding through H2A/H4. Mutation of these residues allowed the generation of doxycycline-inducible (i) separation-of-function IκBα mutants that are specifically deficient in one or the other function, at least in the intestinal epithelial cells³². We called i-IκBα^{ΔChromatin} the i-SOF IκBα mutant that interacts with NF-κB but is deficient for H2A and H4 binding and i-IκBα^{ΔNF-κB} the one that interact with histones but is deficient for NF-κB subunits binding (**Figure 5B** and [32](#)). The three different IκBα forms (i-IκBα^{WT}, i-IκBα^{ΔNF-κB} and i-IκBα^{ΔChromatin}) were stably transfected in the IκBα KO mESCs and induced by 16h of doxycycline treatment (**Figure S4A**). We used these cells to investigate the biochemical properties and functional impact of SOF IκBα mutants in mESCs. By pull-down experiments, we found that i-IκBα^{ΔNF-κB} expressed in ESCs was able to interact with histone H2A but not with the NF-κB member p50. In contrast, i-IκBα^{ΔChromatin} interacts with p50 but not with H2A, while i-IκBα^{WT} preserves both binding capacities (**Figure 5C**). In concordance with these results, i-IκBα^{WT} and i-IκBα^{ΔNF-κB} were found in both the cytoplasmic and chromatin fractions of mESCs, whereas IκBα^{ΔChromatin} was retained in the cytoplasm (**Figures 5D-E**). In multiple experiments, we noticed a significant reduction in protein levels of IκBα^{ΔChromatin} despite the mRNA expression levels of the different IκBα forms being comparable (**Figures 5C-D** and **S4A**).

Then, we studied whether i-IκBα^{WT} and/or the i-SOF IκBα mutants (IκBα^{ΔNF-κB} or IκBα^{ΔChromatin}) were able to reverse any of the phenotypes observed in the IκBα-KO mESCs (**Figure S4B**). Induction of i-IκBα^{WT} and i-IκBα^{ΔNF-κB} reduced the expression levels of the naïve pluripotent genes *Zfp42*, *Klf2*, *Sox2* and *Tbx3*, which were increased by i-IκBα^{ΔChromatin} (**Figure 5F**). In addition, the ground state-associated DNA hypomethylation was specifically reverted in i-IκBα^{WT} and i-IκBα^{ΔNF-κB} mESCs but not in i-IκBα^{ΔChromatin} mESCs (**Figure 5G**). Finally, we addressed whether i-IκBα^{WT}, i-IκBα^{ΔNF-κB} and i-IκBα^{ΔChromatin} mESCs were capable to revert the differentiation blockage of IκBα-KO ESCs (**Figure S4B**). Induction of IκBα^{WT} and IκBα^{ΔNF-κB} was enough to restore the differentiation potential of IκBα-KO mESCs into EBs, as indicated the increase in the number of differentiated cells (based on percentage of SSEA-1^{neg} cells) (**Figures 5H** and **S4C**) and the reduced number of AP+ colonies (in the 216h IκBα-KO reconstituted EB assays), which was similar to the number of colonies obtained from IκBα^{WT} EBs (**Figures 5I**). Lastly, the number of remaining pluripotent-like cells (defined by OCT3/4 NANOG staining) was also reduced in i-IκBα^{WT} and i-IκBα^{ΔNF-κB} 216h EBs, and only small and few regions of undifferentiated cells was observed. In contrast, induction of i-IκBα^{ΔChromatin} did not restore the differentiation potential of IκBα-KO mESCs (**Figures 5J** and **S4D**).

These results demonstrate that the chromatin-dependent IκBα function, but not its NF-κB-related activity, is necessary for the proper regulation of chromatin marks at specific genomic regions that are linked to transcriptional changes that are likely at the base of the capacity of ESCs to exit the ground state of naïve pluripotency and differentiate.

Discussion

Here we have identified a new and unexpected function for the IκBα protein in the regulation of the naïve pluripotency exit. Using mESCs to investigate the role of IκBα in pluripotency maintenance and differentiation, we discovered that the absence of IκBα severely impairs the exit of pluripotency. Furthermore, IκBα-KO mESCs stabilizes the ground state of naïve pluripotency under Serum/LIF conditions, shedding light on its function as a critical regulator of the transition from naïve to primed pluripotency. While IκBα is commonly known for its role as an inhibitor of the NF-κB signaling pathway²⁶, our laboratory has previously furnished compelling evidence of its alternative role through its interaction with histones and other chromatin components^{27,29,31}. We have demonstrated that chromatin-bound IκBα plays a crucial role in regulating skin and intestinal stem cells^{27,28}, hematopoietic stem cell development⁴², and it

influences the regenerative capacity of these tissues, and in some cases, their susceptibility to neoplastic transformation. Disentangling the chromatin-related function of I κ B α from its canonical role as an inhibitor of NF- κ B has been challenging, making it difficult to determine its truly biological significance. To tackle this challenge, we engineered separation-of-function (SOF) mutants of I κ B α , as detailed in [43](#), by identifying specific residues that are essential for binding either NF- κ B elements or histones. Interestingly, we have shown that only the histone-binding proficient I κ B α mutant (I κ B α^{Δ NF- κ B), which lacks the ability to bind to NF- κ B, has the capability to reverse the stabilization of the ground state observed in I κ B α -KO mESCs. This is sufficient to facilitate their exit from the state of naïve pluripotency, restoring their full differentiation potential (**Figure 5**). The involvement of NF- κ B in pluripotency has been a subject of prior investigation. Studies have revealed that pluripotent cells display a dampened inflammatory signaling pathway, which is induced upon pluripotency dissolution and activation of differentiation [24](#), [44](#). However, the precise molecular mechanisms underlying the attenuated status of NF- κ B during this stage remain incompletely understood. A recent work has shed light on a potential regulatory axis involving ATG5- β -TrCP1-NF- κ B, proposing it as a mechanism that diminishes NF- κ B activity by stabilizing the I κ B α protein in mESCs [23](#). In any case, since modification of canonical NF- κ B activity directly impacts on the levels I κ B α expression, the previous NF- κ B-associated phenotypes should be reevaluated considering this chromatin role of I κ B α . Furthermore, the expression of I κ B α^{Δ Chromatin, which retains the inhibitory function of NF- κ B, failed to mitigate the ground state stabilization observed in I κ B α -KO mESCs (**Figure 5**). This finding suggests that the observed role of I κ B α in regulating the exit from naïve pluripotency is not due to NF- κ B inhibition. In fact, there is evidence that the chromatin function of I κ B α is an ancestral function preceding its role as NF- κ B inhibitor. In *Caenorhabditis Elegans* (*C.elegans*), which lacks NF- κ B orthologs but possesses two homologs of I κ B α , the absence of I κ B α orthologs has severe multi-organ differentiation defects [39](#). This observation further supports the notion that the chromatin-related function of I κ B α plays a fundamental role in developmental processes, independent of its canonical role in NF- κ B signaling.

We have observed that I κ B α -KO mESCs exhibit epigenetic and transcriptomic profiles resembling the ground state of naïve pluripotency under Serum/LIF culture (**Figure 3**). In this regard, the fact that I κ B α is preferentially located in the chromatin of mESCs cultured in Serum/LIF, when they exhibit a high degree of heterogeneity, suggests that I κ B α might act as a regulator of this heterogeneity. One potential explanation might be that I κ B α could be affecting the stability of fluctuating transcription factors, which is crucial to mediate the pluripotent-to-differentiation balance [3](#). Thus, the lack of I κ B α might stabilize those transcription factors that would favor the ground-state observed in I κ B α -KO mESCs cultured in Serum/LIF. Further experiments are required to demonstrate this hypothesis. Moreover, the differences in murine and human pluripotency [11](#) point out the necessity to address the real impact of I κ B α modulation in the stabilization of the ground state in human pluripotent stem cells.

In summary, our work establishes that I κ B α mediates the exit from naïve pluripotency by modulating the activation of naïve pluripotency genes. Importantly, this newly identified role of I κ B α operates independently of its canonical function in inhibiting the NF- κ B pathway. Our findings underscore the intricate interplay between inflammation and pluripotency status, revealing a previously unrecognized complexity in their interaction.

Methods

Cell culture

mESC line ES-E14TG2a (ATCC; Cat #CRL-1821) was cultured on plastic dishes precoated with 0.1% (w/v) Gelatin (Sigma; Cat #G2500-100G) in Serum/LIF medium. Serum/LIF is composed by DMEM basal medium (Sigma-Aldrich; Cat #D5796) supplemented with 15% FBS (ESC-qualified; Gibco Cat

#26140079), 1X Glutamax (Gibco; Cat #35050061), 1X NEAA (Gibco; Cat#11140050), 1mM Sodium Pyruvate (Gibco; Cat#11360070), 1000U/mL Leukemia Inhibitory Factor (LIF) (Millipore, Cat #ESG1107) and 0.125mM 2-mercaptoethanol (Gibco; Cat#31350010). Medium was changed every day, and cells were splitted every other day using TrypLE Express (Gibco; Cat #12605010) for harvesting. Cells were maintained in a 5% CO₂ incubator at 37°C.

For inducing the ground-state of naïve pluripotency, mESCs were cultured in 2i/LIF medium for 2 consecutive passages. 2i/LIF medium is composed by N2i medium (TAKARA, Cat #Y40002) supplemented with 1000U/mL LIF, 0.4 µM PD032591 (Selleck Chemicals, Cat #S1036) and 3 µM CHIR99021 (Merck, Cat #SML1046).

Epiblast stem cell differentiation

Differentiation from mESCs towards Epiblast Stem Cells (EpiSCs) was performed as previously described⁴⁵. 3x10⁴ mESCs were seeded in 6-well plastic dishes, and they were cultured in Serum/LIF medium for 24h. Medium was then switched to N2i medium (TAKARA, Cat #Y40002) supplemented with 20 ng/ml activin A (Cat. #120-14E; PeproTech) and 10 ng/ml Fgf basic (R&D Systems, Cat #233-FB-025/CF). Cells were submitted to daily media changes till day 5 (120h), when they were further analyzed.

Embryoid bodies differentiation from mESCs

Embryoid bodies differentiation was established as described in⁴⁶. Briefly, mESCs were splitted twice in Serum/LIF medium before inducing differentiation. Once mESCs are 80% confluent, cells were collected using TrypLE Express. One well of 6-well plate was splitted in an entire 6-well plate in IMDM-ES medium for 48h. IMDM-ES medium is composed of Iscove's Modified Dulbecco's Medium (IMDM) (Cytiva, Cat #16SH30259.01) supplemented with 20% FBS (ESC-qualified; Gibco Cat #26140079), 1X Glutamax (Gibco; Cat #35050061), 1X NEAA (Gibco; Cat#11140050), 1mM Sodium Pyruvate (Gibco; Cat#11360070), 10ng/mL Leukemia Inhibitory Factor (LIF) (Millipore, Cat #ESG1107) and 0.125mM 2-mercaptoethanol (Gibco; Cat#31350010). For embryoid body induction, mESCs were harvested, and they were rinsed twice with DPBS (Gibco; Cat #14190144). Cells were very well disaggregated into single-cells, and 1.2 x 10⁴ cells/mL embryoid body differentiation (EB^{diff}) medium were resuspended to a total volume of 25mL of EB^{diff} medium. EB^{diff} medium is composed by IMDM supplemented with 15% FBS (ESC-qualified; Gibco Cat #26140079), 1X Glutamax (Gibco; Cat #35050061), 50 µg/mL ascorbic acid (Sigma; Cat #A-4544), 180 µg/mL Transferrin (Roche; Cat #10652202001) and 0.45 mM alpha-monothioglycerol (MTG) (Sigma; Cat #M6145). EBs were formed in suspension for 5 days (120h). At day 5, in order to elongate the differentiation up to 216h (day 9), EB^{diff} medium was refreshed by harvesting EBs with 10mL serological pipette, centrifuge at 200 g for 3 min and EBs were resuspended in fresh EB^{diff} medium for 4 more days.

CRISPR/Cas9 gene editing and cell lines generation in mESCs

The two guide RNAs (gRNAs) targeting the Nfkb locus were designed using the CRISPR design tool from MIT (<http://crispr.mit.edu>). The best 2 gRNAs (based on on-target and off-target scores) that were targeting the exon 1 of Nfkb (IκBα gene) were selected. After annealing, one of the gRNAs was cloned into SpCas9(BB)-2A-GFP (px458) plasmid (Addgene; Cat #48138), and the other gRNA was cloned into the px330-mCherry plasmid (modified from Addgene; Cat #98750 to incorporate mCherry reporter). mESCs were co-transfected with the two plasmids (px458-gRNA1 and px330-mCherry-gRNA2). 3x10⁵ cells were seeded a day before per well of 6-well plate. At day of transfection, cells were washed once with 1X DPBS (Gibco; Cat #14190144), and 2mL Opti-MEM medium (Gibco; Cat #31985070) was added into cells. 1.25 µg of each plasmid (2.5 µg of total DNA) was incubated with 10 µL of Lipofectamine 2000 (Invitrogen; Cat #11668019) in 240 µL of Opti-MEM for 20 min. OptiMEM::Lipofectamine::DNA mixture was added into mESCs, and cells were incubated for 5 hours. Cells were then washed with DPBS, and medium was replaced by

Serum/LIF. 48h after transfection, GFP⁺ mCherry⁺ single cells were sorted by FACS using BD FACS Aria II Cell Sorter (BD Bioscience). Mutant clones were screened through PCR and western blotting to identify single clones with no IκBα protein expression. Non-targeting scrambled gRNAs were cloned into px458 and px330-mCherry plasmids as wildtype clones. Three independent clones from each genotype (IκBα-WT and IκBα-KO) were selected for further experiments.

Doxycycline-inducible IκBα (IκBα^{WT}, IκBα^{ΔNF-κB} and i-IκBα^{ΔH2A/H4}) mESCs were generated by cloning the three different IκBα versions into a PiggyBac transposon system⁴⁷, IκBα protein-coding cDNAs were PCR-amplified, and NheI and SalI restriction sites were placed at the 5' and 3' ends, respectively. T2A-EGFP fragment was amplified from PX458 plasmid, and SalI and AgeI restriction sites were introduced at its 5' and 3' ends. PB-TRE backbone (Addgene, Cat# 63800) was digested with NheI and AgeI enzymes, and mNfκbia and T2A-EGFP fragments were ligated into the PB-TRE digested vector. To generate mESCs containing the inducible vector, IκBα-KO mESCs were co-transfected with PB-TRE-mNfκbia-T2A-EGFP and PiggyBac transposase plasmids, and pool of transfected cells was selected by Hygromycin (100μg/mL) for 7 days. Cells were doubly screened by FACS sorting green fluorescent protein after 24h of doxycycline (1μg/mL) treatment. Pool of cells were used for further experiments. Oligos sequences are included in supplementary table 1.

Teratoma formation assay

IκBα-WT and IκBα-KO mESCs grown in Serum/LIF (5×10^5) were injected intramuscularly into severe combined immunodeficient mice (NSG). In order to favor 3D aggregation of cells and teratoma formation, cells were resuspended in Matrigel Matrix (BD; Cat #356234) prior to injection. Six weeks later, mice with tumors were euthanized, and tumors were fixed in formaldehyde, embedded in paraffin, sectioned and stained with hematoxylin and eosin for histological analysis.

Immunofluorescence staining

For immunostaining of mESCs, cells were seeded on 0.1% gelatin-coated coverslips on 6-well plates; for EB immunofluorescence, they were collected directly from the plate. Samples were washed twice with 1X PBS, and they were fixed at 4°C for 30 minutes with 4% PFA (Electron Microscopy Sciences; Cat #15713S). For immunofluorescence of 5-Methylcytosine (5mC), fixed cells were incubated with 2M Hydrochloric Acid (Sigma-Aldrich, Cat #H1758) for 20 minutes at room temperature. Samples were then washed twice with 1X Tris-buffered saline (TBS; 50 mM Tris-Cl, pH 8) and permeabilized and blocked with 1X TBS supplemented with 1% Triton-X100 (MERCK; Cat #9036-19-5) and 6% FBS (Biological Industries; Cat #04-001-1A) for 2h at 4°C. Samples were washed twice with 1X TBS supplemented with 6% FBS. Primary antibody incubation was performed in 1X TBS plus 6% FBS and 0.3% or 0.5% Triton-X100 (0.3% for 2D culture and 0.5% for EBs) overnight at 4°C. The following primary antibodies were used: OCT3/4 (1:250; Santa Cruz; Cat #sc-5279), NANOG (1:250; Novus Biologicals; Cat #NB100-588), 5-Methylcytosine (1:500, Invitrogen, Cat #MA5-24694), H3K27Ac (1:2000, Abcam, Cat #AB4729). Samples were then washed 4 times with 1X TBS, 5 min each washing. Secondary antibody incubation was performed in TBS 1X plus 1% BSA (Sigma-Aldrich; Cat #9048-46-8) for 2h at room temperature. The following antibodies were used: Alexa Fluor 488 donkey anti-mouse antibody (1:1000; Invitrogen; Cat #A-21202), Alexa Fluor 647 donkey anti-mouse antibody (1:1000; Invitrogen; Cat #A-31571), Alexa Fluor 594 donkey anti-rabbit antibody (1:1000; Life Technologies; Cat #A-21207), Alexa Fluor 647 donkey anti-rabbit antibody (1:1000, Invitrogen; Cat #A-31573). Samples were washed three times with 1X TBS for 5 min at room temperature each rinse. Samples were mounted using DAPI Fluoromount-G (Southern Biotech; Cat #0100-20).

Microscopy and image acquisition

Fluorescence images were acquired using Confocal Leica TCS SP5 (Leica Microsystems), and Leica application software LAS AF (Leica Microsystems) was used to visualize the images. Images of teratoma haematoxylin and eosin and immunohistochemistry stainings were acquired using BX61 Olympus Microscope (Olympus), and PRECiV™ 2D Image and Measurement Software (Olympus) was used to visualize the images. The Image J (version 1.15) was used for further analysis ⁴⁸.

Flow cytometry sample preparation and analysis

Cells were collected and they were purified based on FACS using BD FACSAria II Cell Sorter (BD Bioscience). Cells were sorted at 3,500 events/second, and at maximum flow rate of 4 and 85 μ m nozzle. 5 μ g/ml of DAPI (Biotium; Cat #BT-40043) was used as a viability dye. For flow cytometry analysis of pluripotency exit, cells were disaggregated using TrypLE Express, and they were incubated at 4°C for 20 minutes with SSEA1-eFluor 660 Monoclonal Antibody (1:200, Invitrogen, Cat #50-8813-42). BD LSRFortessa Cell Analyzer or BD LSR II Flow Cytometer (BD Bioscience) were used for Flow Cytometry Analysis experiments. Flow cytometry data were analyzed using FlowJo X v10.0.7 (BD Biosciences).

RNA isolation, cDNA synthesis and quantitative RT-PCR

Total RNA isolation from cells was performed using the RNeasy Plus Mini Kit (Qiagen; Cat #74136) or RNeasy Micro Kit (Qiagen; Cat #74004) following manufacturer's instructions. Amount of RNA was quantified with Nanodrop (Thermo Fisher; Cat #ND2000CLAPTOP), and 2 μ g of total RNA was retro-transcribed using Transcriptor First Strand cDNA Synthesis Kit (Roche; Cat #04897030001) following the manufacturer's instructions.

Quantitative RT-PCR was performed in triplicates for each sample, and SYBR Green I Master Kit (Roche; Cat #04887352001) was used to carry out the reaction. qRT-PCR was performed using the LightCycler 480 system (Roche). Relative expression levels were calculated as $2^{-\Delta CT}$ normalized with the average CT of the housekeeping gene Tbp or Gapdh. Oligos sequences are found in supplementary table 1.

Chromatin Immunoprecipitation (ChIP)

$4\text{--}6 \times 10^7$ mESCs were cross-linked by incubating them in DPBS (Gibco, Cat #14190094) supplemented with 1% formaldehyde (Sigma-Aldrich; Cat #252549) for 10 min rocking at room temperature. Cross-linking was stopped using 125 mM Glycine (Sigma-Aldrich, Cat #G8790) rocking for 5 minutes at room temperature. Fixed cells were then washed twice with ice-cold DPBS, and scrapped and collected using DPBS supplemented with protease/phosphatase inhibitor cocktail composed by 1X cOmplete™, EDTA-free Protease Inhibitor Cocktail (Roche, Cat #11873580001), 1 mM PMSF, 1mM Sodium Orthovanadate and 20 mM β -Glycerol phosphate. Cells were centrifuged at 3200g for 5 minutes at 4°C. Cells were lysed by resuspending cell pellet in ice-cold ChIP buffer (1 volume of SDS buffer [100mM NaCl, 50mM Tris-HCl pH 8.1, 5mM EDTA pH 8, 0.5% SDS] and 0.5 volume of triton dilution buffer [100mM Tris-HCl pH 8.6, 100mM NaCl, 5mM EDTA pH 8, 5% Triton X-100]) supplemented with protease/phosphatase inhibitor cocktail, and samples were sonicated using sonication beads (Diagenode; Cat #C01020031) and the Bioruptor Pico Sonicator (Diagenode; Cat #B01060010) for 20 cycles (each cycle 30 seconds on/30 seconds off) or till DNA fragments have 100-300bp size. Samples were centrifuged at 16000g for 20 minutes at 4°C. Chromatin was quantified, and 30 μ g of chromatin was incubated with every 5 μ g of antibody rotating for 16 hours (or overnight) at 4°C. The following antibodies were used: H3K4me3 (Abcam, Cat #ab8580), H3K27me3 (Millipore, Cat #07-449), H3K27Ac (Abcam, Cat #ab4729), H3K4me1 (Abcam, Cat #ab8895). Samples were pulled down by incubation with Protein A-Sepharose™ CL-4B (previously hydrated and blocked with 0.05% BSA) for 3h at 4°C in rotation. Sample was washed with a low salt washing buffer (50mM HEPES pH 7.5, 140mM NaCl and 1% Triton) three times, one

wash with a high salt wash buffer (50mM HEPES pH 7.5, 500mM NaCl and 1% Triton) and one wash with TE pH 8 (10mM Tris-HCl pH8, 1mM EDTA). Samples were then eluted in 1% SDS and 100mM NaHCO₃. Samples were descrosslinked by incubating for 16 hours (or overnight) at 65°C shaking at 450 rpm, and were treated with Proteinase K for 1h at 45°C. DNA was purified using QIAquick PCR Purification Kit (Qiagen, Cat #28106), following the manufacturer's instructions.

For ChIP followed by sequencing (ChIP-seq) Purified DNA concentration and integrity were determined using Agilent Bioanalyzer (Agilent Technologies; Cat #G2939BA). Libraries were prepared using standard protocols. Chromatin was sequenced using Illumina HiSeq platform (Illumina, Inc.) (50bp single-end reads). Samples sequencing depth range was the following: (i) H3K4me3: 2.56-2.74x10⁷ reads, (ii) H3K27me3: 6.19-7.2x10⁷ reads, (iii) H3K27Ac: 9.11-10.65x10⁷ reads and (iv) H3K4me1: 9.76-10.58x10⁷ reads.

ChIP-seq data analysis

Quality control was performed on raw data with FASTQC tool. Raw reads were trimmed to remove adapters presence with Trimgalore (v0.6.6) ⁴⁹. Default parameters were used except for a minimum quality of 15 (Phred score) and an adapter removal stringency of 3bp overlap. For H3K4me3, H3K27me3 and H3K4me1 data, trimmed reads were aligned to the reference genome with Bowtie2 (v2.4.4) which was executed with default parameters ⁵⁰. Required genome index was built with corresponding GRCm38 fasta file retrieved from Ensembl (<http://ftp.ensembl.org/pub/release-102/>). Multmapped reads and those exhibiting MAPQ < 20 were removed. Randomly placed multi mappers were removed from the mapped reads. For all cases, duplicated reads were marked with SAMtools (v1.15) ⁵¹. Drosophila Melanogaster spike-ins, present in H3K27me3, were discarded. NSC and RSC quality metrics were computed with PhantomPeakQualTools (v1.2) ⁵². ENCODE blacklisted regions (mm10 v2) were removed prior to peak calling. BigWig files were individually generated using deepTools (v3.5.1) bamCoverage with -ignoreDuplicates -binSize 10 -smoothLength 30 -effectiveGenomeSize 2308125349 -normalizeUsing RPGC and -extendReads *Fragment_Length* options ⁵³. The effective genome size was particularized to a read length of 50bp and directly retrieved from deepTools web site (<https://deeptools.readthedocs.io/en/develop/content/feature/effectiveGenomeSize.html>). *Fragment_Length* was retrieved from PhantomPeakQualTools results. For all histone marks except for H3K4me3, peak calling was conducted by means of epic2 (v0.0.52) with -effective-genome-fraction 0.8452 -fragment-size *Fragment_Length* options and chromosome sizes only referring to canonical chromosomes ⁵⁴. For H3K4me3, MACS2 (v2.2.7.1) was used to identify peaks with -nomodel -extsize *Fragment_Length* -g 2308125349 options ⁵⁵. The corresponding input sample was used in all peak calling computations. For the histone marks, peaks were called with adjusted p-values (FDR) < 0.05.

Peak annotation was performed with ChIPseeker R (v4.2.1) package (v1.34.1) considering a TSS region range between 5000 bp upstream and 100 bp downstream (Yu et al., 2015). Required TxDb object was generated from the Ensembl GRCm38 gtf file retrieved (<http://ftp.ensembl.org/pub/release-102/>). A consensus peakset was obtained from the three biological replicates per histone mark and condition (IkBa-WT or IkBa-KO) by identifying overlapping peaks in at least two out of the three replicates.

Differential binding analysis (DBA) was conducted with DiffBind (v3.8.4) per histone mark ⁵⁶. Default parameters were used except for the summits parameter which was set to 500bp for all histone marks except for H3K4me3 (150bp) in order to consider, for testing, intervals of 1000bp or 300bp respectively. Summit values were selected to have interval widths between the minimum and first quartile peak width values for each histone mark. EdgeR was the statistical method used for all the three analyses. Differentially bound regions (DBRs) between IkBa-KO and IkBa-WT samples were called with adjusted p-values (FDR) < 0.05. Identified DBRs with any annotated gene were plotted with EnrichedHeatmap R package (v1.18.1) ⁵⁷. To summarize replicates per

condition, `normalizeToMatrix` function was used based on corresponding BigWig files in `w0` mean mode in 50bp windows. Tracks visualization were obtained by means of Integrative Genomics Browser (IGV) tool ⁵⁸.

Enhancers activity identification

Consensus peaksets derived from the three H3K27ac and H3K4me1 IkBa-WT mESCs replicates were used to identify poised and active enhancers in an IkBa-WT scenario. Putative poised enhancers were defined as those regions with H3K4me1 but no H3K27ac peaks. Putative active enhancers were defined as those regions with H3K27ac and presence/absence H3K4me1 peaks. To assess any differential enhancers activity in IkBa-KO vs IkBa-WT mESCs cultured in Serum/LIF, differentially bound regions and consensus peaksets (IkBa-KO) identified in H3K4me1 and H3K27ac were required. Putative gained or lost poised/active enhancers in $\text{IkBa}^{-/-}$ were obtained with following criteria: (i) for gained/lost poised enhancers in $\text{IkBa}^{-/-}$: a differential H3K4me1 increase/decrease and absence of H3K27ac peaks in $\text{IkBa}^{-/-}$ consensus peakset, (ii) for gained/lost active enhancers (without H3K4me1) in IkBa-KO : a differential H3K27ac increase/decrease and absence of H3K4me1 in IkBa-KO consensus peakset and (iii) for gained/lost active enhancers (with H3K4me1) in IkBa-KO : a differential H3K27ac increase/decrease and presence of H3K4me1 in $\text{IkBa}^{-/-}$ consensus peakset.

A maximum gap of 1000bp was allowed for checking the overlap between two different histone marks. For this purpose, the ‘`subsetByOverlaps`’ function from the `IRanges` R package was used (v.2.34.1).

RNA-seq experiments

Total RNA from three independent clones from mESCs, 48h EBs and 96h EBs was isolated using the RNeasy Plus Mini Kit (Qiagen; Cat #74136) following manufacturer’s instructions. Amount of RNA was quantified with Nanodrop (Thermo Fisher; Cat #ND2000CLAPTOP), and RNA integrity was addressed by agarose gel and Agilent Bioanalyzer (Agilent Technologies; Cat #G2939BA). Libraries sequenced using Illumina HiSeq 2500 (Illumina, Inc.) (125bp paired-end reads). Samples sequencing depth ranged between 35M and 52M reads (average 41M reads) per sample.

RNA-seq data analysis

Quality control was performed on raw data with the FASTQC tool (v0.11.9). Raw reads were trimmed to remove adapter presence with Trimalore (v0.6.6) ⁴⁹. Default parameters were used except for a minimum quality of 15 (Phred score) and an adapter removal stringency of 3bp overlap. Trimmed reads were aligned to reference the genome with STAR aligner tool (v2.7.8). STAR was executed with default parameters except for the number of allowed mismatches which was set to 1. Required genome index was built with corresponding GRCm38 gtf and fasta files retrieved from Ensembl (<http://ftp.ensembl.org/pub/release-102/> ⁵⁹). Obtained BAM files with uniquely mapped reads were considered for further analysis. Raw gene expression was quantified using featureCounts tool from subRead software (v2.0.1) with exon as feature ⁵⁹. The raw counts matrix was imported into the R Statistical Software environment (v4.2.1) for downstream analysis. Raw expression matrix included 55,487 genes per 18 samples in total. Experimental design considered three timepoints: mouse ESCs, EBs at 48h and EBs at 96h. Each time point included 6 samples distributed in two conditions: 3 IkBa-WT and 3 IkBa-KO . Prior to statistical analysis, those genes with less than 10 raw counts across the 6 samples under test were removed. After pre-filtering, 21,843 genes (mESCs), 21,424 genes (EBs 48h) or 21,664 genes (EBs 96h) were available for testing. For visualization purposes, counts were normalized by the variance-stabilizing transformation method as implemented in DESeq2 R package ⁶⁰ (v1.38.3). Differential expression analysis (DEA) was conducted with DESeq2. Each time point was independently analyzed. Fitted statistical model included sample conditions as covariable with IkBa-WT as the reference. Obtained log2 fold change values were shrunk with apeglm shrinkage estimator R

package (v1.20.0) ⁶¹. Raw p-values were adjusted for multiple testing using the Benjamini-Hochberg False Discovery Rate (FDR) ⁶². Differentially Expressed Genes (DEGs) between IκBα-KO and IκBα-WT samples were called with adjusted p-values (FDR) < 0.05 and absolute shrunken log₂ Fold change > 1. Data visualization was performed with the ggplot2 (v3.4.1).

Genome-wide DNA methylation samples preparation

DNA from frozen mESCs pellets was extracted using DNeasy Blood and Tissue Kit (Qiagen GmbH, Hilden, Germany). Purified genomic DNA was quantified with Qubit (Invitrogen, Carlsbad, CA, USA) according to manufacturer's instructions. Infinium Mouse Methylation BeadChip (Illumina, Inc., San Diego, CA, USA) arrays were used to profile DNA methylation genome wide. This platform allows over 285,000 methylation sites per sample to be interrogated at single-nucleotide resolution. The samples were bisulfite converted using EZ DNA Methylation-Gold™ Kit (Zymo Research, CA, USA) and were hybridized in the array following the manufacturer's instructions.

DNA methylation data analysis

The DNA methylation profile of the studied samples was assessed using the Infinium Mouse Methylation BeadChip Array (~285,000 methylation sites) as previously described ⁶³. Briefly, raw signal intensities were obtained with GenomeStudio Software 2011.1 (Illumina) and DNA methylation beta values were computed from raw IDAT files using GenomeStudio default normalization with control probes and background subtraction. Quality control steps to remove erratic probe signals were performed within the R statistical environment (v4.0.3). We removed probes with detection p value > 0.01, genotyping probes and manufacturing flagged (MFG) probes described in the Illumina manifest file (<https://support.illumina.com/downloads/infinium-mouse-methylation-manifest-file.html>). The differentially methylated probes (DMPs) between IκBα-WT and IκBα-KO samples were computed separately for each time point (mESCs and EBs at 96h) by deriving a linear model with the limma R package (v3.46.0). Each condition included 3 samples per time point. DMPs with adjusted p-value (FDR) < 0.05 and absolute mean methylation beta value difference between conditions > 0.3 were considered significant. DNA methylation analysis was performed using the mm10 mouse genome reference build and the complete annotation was downloaded from the annotated manifest file (<http://zwdzwd.github.io/InfiniumAnnotation#mouse>) ³⁶.

Functional analysis

Overrepresentation analysis was applied over lists of selected genes derived from RNA-seq data (DEGs) or from ChIP-seq data (differentially bound regions). The Gene Ontology (Biological Process ontology, GO BP terms), KEGG PATHWAY and WikiPathways databases for Mus Musculus ^{64–66} were interrogated by means of clusterProfiler R package (v4.6.2) (Wu et al., 2021). Corresponding Entrez identifiers were used. Benjamini-Hochberg procedure was used to obtain adjusted p-values. Obtained GO BP terms were simplified using the simplify function from clusterProfiler with default parameters. Overrepresented terms or processes were called with adjusted p-values (FDR) < 0.05.

Gene Set Enrichment Analysis (GSEA) was performed for mESCs against the three cell states signatures defined by other authors ⁶⁷. Briefly, each signature was composed of 200 genes uniquely expressed in each state obtained from bulk RNA-seq performed per state. For this purpose, the complete list of genes from mESCs samples (21,843 genes) was ranked based on the shrunken log₂ Fold Change obtained from DEA. GSEA was conducted through the fgseaMultilevel function from fgsea R package (v1.24.0) ⁶⁸ with default parameters. Enrichment plots were generated with the same package.

Additionally, the testEnrichment function from SeSAmE R package (v1.14.2) ⁶⁹ was used for conducting functional analysis with default parameters over the list of DMPs. Probe design, transcription factor binding site and histone modifications consensus database sets, included in the same package, were interrogated.

Gene Set Variation Analysis (GSVA) R package (v1.46.0) with default parameters were used to obtain Z-score values for genes annotated to endoderm (GO:0001706), mesoderm (GO:0001707) and ectoderm (GO:0001705) GO BP terms ⁷⁰.

Statistical analysis

Statistical analysis was performed with GraphPad Prism v.8.0.1. (GraphPad Software, Inc.). Unless specified, the comparison between two groups was performed with unpaired two-sided t-test. A p-value < 0.05 was considered significant.

Data availability

All sequencing data is deposited at GEO under a SuperSeries with the accession number GSE239565)[<https://www.ncbi.nlm.nih.gov/geo/query/acc.cgi?acc=GSE239565>]. Individual SubSeries can be found at: GSE239563 (RNA-seq data), GSE239564 (ChIP-seq data) and GSE239562 (Methylation array data).

Acknowledgements

We would like to acknowledge all members of the Bigas/Espinosa labs for helpful discussions. We are grateful for technical support to CRG/UPF Flow Cytometry Unit, CRG Genomics and Advanced Light Microscopy Units. This work has been supported by Spanish Ministry of Science and Innovation (PID2019-104695RB-I00, PLEC2021-007518, PDC2021-120817-I00), Generalitat de Catalunya (2021SGR 39) and Departament de Salut (SLT002/16/00299) to AB; the Spanish Ministry of Science and Innovation (PID2019-108322GB-I00 and PID2022-142679NB-I00) to LDC; the Spanish Ministry of Science and Innovation (PID2021-123383NB-I00.) and the Agència de Gestió d'Ajuts Universitaris i de Recerca (2021 SGR 01222) to BP. L.G.P has been a recipient of FI AGAUR fellowship (2019 FI-B 00151/2020 FI_B1 00130) from Generalitat de Catalunya. D.A-V was funded by the FIS fellowship (FI20/00130) from Instituto Carlos III. M.B. received funding from the Ramón Areces Foundation. M.M. is a recipient of a grant from the Instituto Carlos III, grant number CA22/00011 (co-funded by the European Social Fund Plus, ESF+ and by the European Union).

Additional information

Code availability

Scripts used to process the generated bulk RNA-seq and ChIP-seq data are available in Github repository: https://github.com/BigasEspinosaLab/PAPER_IkBa_Naive_Pluripotency

Author contribution

L.G.P, L.E and A.B designed the study. L.G.P, D.A-V, M.B, A.I, J.G, J.B, D.A.E, C.A.G.P, C.B, V.R.C and A.V performed experiments. L.G.P, M.M, M.B and C.A.G.P performed bioinformatics analysis. L.G and A.B wrote the manuscript with input from all authors. C.B, A.V, A.V, P.M, L.D.C, G.S, B.P, M.E and L.E provided input on experimental design. L.E and A.B provided resources and supervised the research.

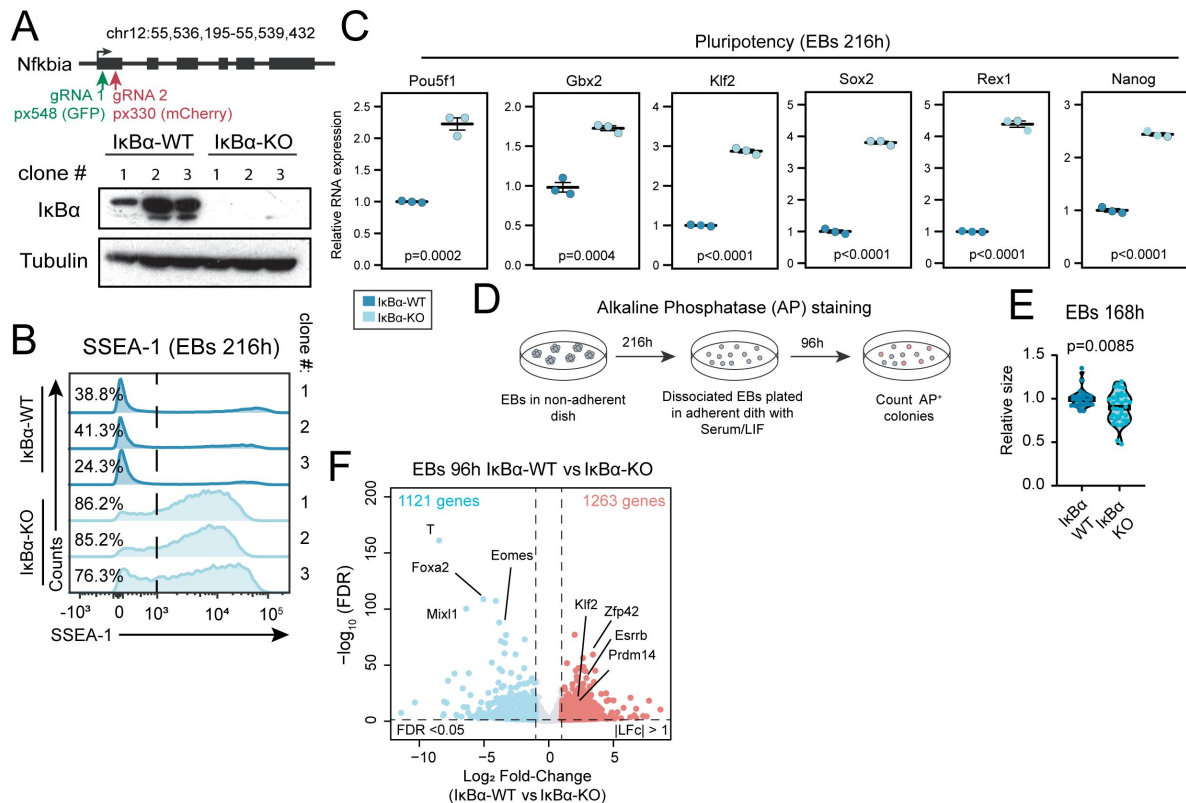


Figure S1.

Depletion of *IκBα* in mESCs compromises the exit from pluripotency. Related to Figure 2.

A. Schematic of the approach followed to deplete *IκBα* protein in mESCs (upper panel) and western blot analysis of three independent *IκBα*-WT and *IκBα*-KO mESC clones (bottom panel). **B.** Flow cytometry plots of SSEA-1 from *IκBα*-WT or *IκBα*-KO EBs 216h. **C.** Relative RNA levels (based on qPCR experiments) of naïve pluripotency genes (*Pou5f1*, *Gbx2*, *Klf2*, *Sox2*, *Rex1*, *Nanog*) in *IκBα*-WT or *IκBα*-KO 216h EBs. RNA levels were normalized based on *Tbp* expression relative to *IκBα*-WT. Each dot represents an independent clone either from *IκBα*-WT or *IκBα*-KO genotypes. Unpaired two-sided t-test was applied. **D.** Schematic of Alkaline Phosphatase (AP) staining carried out in EBs. *IκBα*-WT or *IκBα*-KO 216h EBs were dissociated and seeded in Serum/LIF medium for another 96h. Attached cells were screened for AP⁺ total cell number. **E.** Violin plot and individual values showing the quantification of relative size of 168h EBs. Each dot represents an embryoid body. Unpaired two-sided t-test was applied. **F.** Volcano plot from differential expression analysis between *IκBα*-KO vs *IκBα*-WT 96h EBs. Dashed vertical lines represent an absolute shrunken log₂ Fold Change = 1 and dashed horizontal line represents an adjusted p-value = 0.05 (FDR).

Figure S2.

Absence of I κ B α favors the ground-state of naïve pluripotency in Serum/LIF conditions. Related to Figure 3.

A. Brightfield images of I κ B α -WT or I κ B α -KO EpiSCs at 120h. Each picture corresponds to an independent clone from either I κ B α -WT or I κ B α -KO genotypes. **B.** Bright-field microscopy images of I κ B α -WT and I κ B α -KO mESCs cultured in Serum/LIF conditions. Two independent clones from each genotype are shown. **C.** DNA methylation levels (mean β -values) across chromosomes in I κ B α -WT vs I κ B α -KO mESCs.

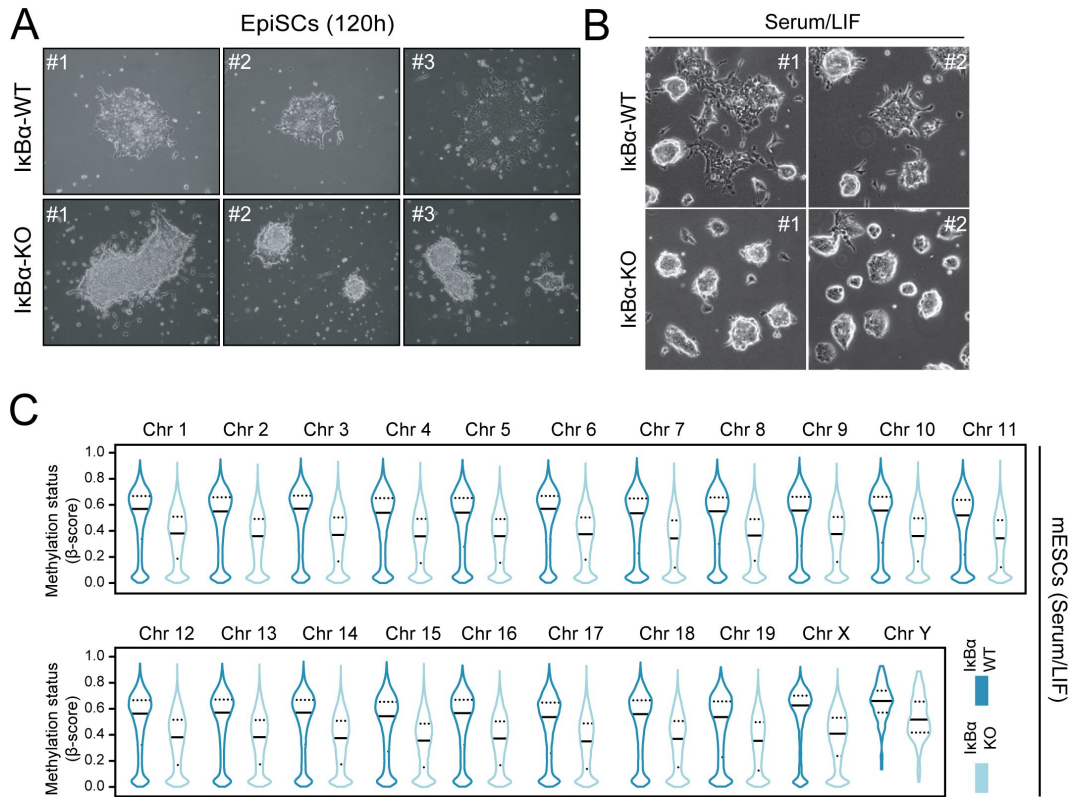
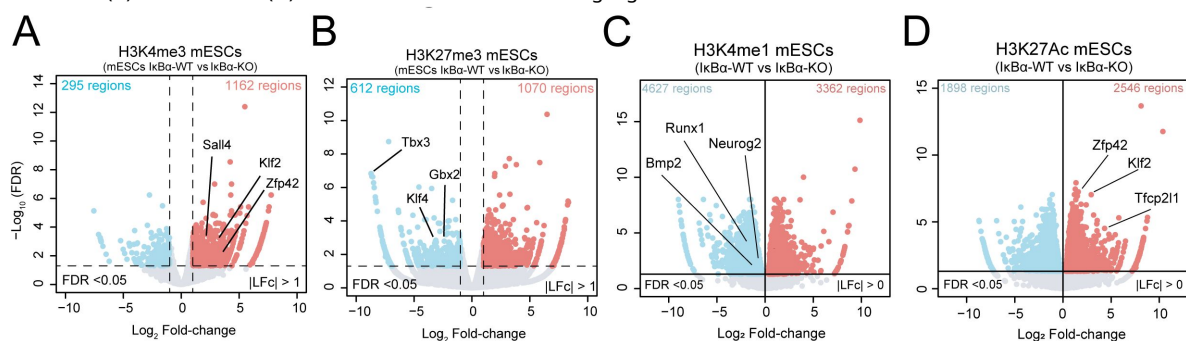


Figure S3.

Epigenetic rewiring characterization in I κ B α -KO mESCs cultured in Serum/LIF. Related to Figure 4. A-D.

Volcano plots from differential binding analysis of H3K4me3 (A), H3K27me3 (B), H3K4me1 (C) and H3K27Ac (D) in I κ B α -WT vs I κ B α -KO mESCs cultured in Serum/LIF. Representative genes with enriched or reduced levels of H3K4me3 (A), H3K27me3 (B), H3K4me1 (C) and H3K27Ac (D) marks in I κ B α -KO mESCs are highlighted.



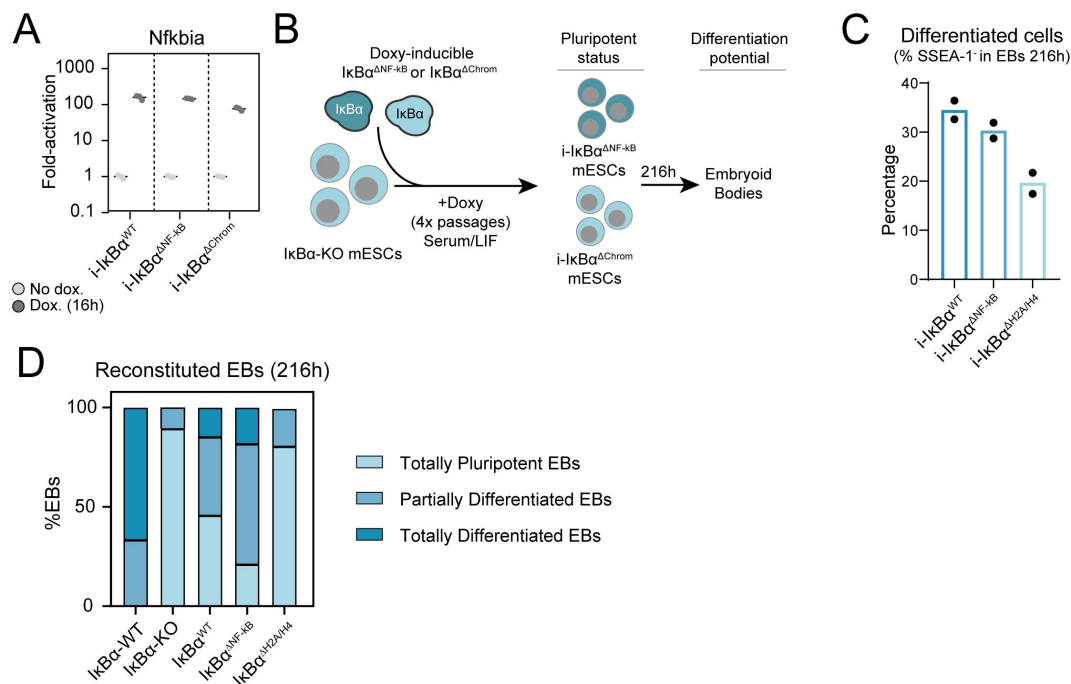


Figure S4.

Reversion of IkBα-KO-related hyper pluripotent status is NF-κB independent. Related to Figure 5.

A. Relative expression level of Nfkb1a gene after overnight doxycycline induction in i-IkBα^{ΔWT}, i-IkBα^{ΔNF-κB} and IkBα^{ΔChrom} mESCs. **B.** Schematic representation of reconstitution of IkBα-KO mESCs with either of the two doxycycline-inducible SOF mutants (i-IkBα^{ΔNF-κB} or IkBα^{ΔChrom}). mESCs were then kept in Serum/LIF medium supplemented with 1μg/mL Doxycycline for 4 consecutive passages. mESCs were characterized at the pluripotent level and then their potential to be further differentiated was addressed. **C.** Percentage of differentiated cells (determined as SSEA-1⁺) at 216h EBs 216h derived from i-IkBα^{ΔWT}, i-IkBα^{ΔNF-κB} and IkBα^{ΔChrom} mESCs. **D.** Quantification of EB differentiation status (percentage of pluripotent cells) at 216h after induction of SOF IkBα mutants. Data from three independent experiments.

References

1. Festuccia N., Osorno R., Wilson V., Chambers I (2013) **The role of pluripotency gene regulatory network components in mediating transitions between pluripotent cell states** *Curr. Opin. Genet. Dev* **23**:504–511
2. Graf T., Stadtfeld M (2008) **Heterogeneity of embryonic and adult stem cells** *Cell Stem Cell* **3**:480–483
3. Martinez Arias A., Brickman J.M. (2011) **Gene expression heterogeneities in embryonic stem cell populations: origin and function** *Curr. Opin. Cell Biol* **23**:650–656
4. Pera M.F., Rossant J (2021) **The exploration of pluripotency space: Charting cell state transitions in peri-implantation development** *Cell Stem Cell* **28**:1896–1906
5. Wang X., Wu Q (2022) **The Divergent Pluripotent States in Mouse and Human Cells** *Genes* **13** <https://doi.org/10.3390/genes13081459>
6. Ying Q.-L., Wray J., Nichols J., Batlle-Morera L., Doble B., Woodgett J., Cohen P., Smith A (2008) **The ground state of embryonic stem cell self-renewal** *Nature* **453**:519–523
7. Marks H. *et al.* (2012) **The transcriptional and epigenomic foundations of ground state pluripotency** *Cell* **149**:590–604
8. Boroviak T., Loos R., Lombard P., Okahara J., Behr R., Sasaki E., Nichols J., Smith A., Bertone P (2015) **Lineage-Specific Profiling Delineates the Emergence and Progression of Naive Pluripotency in Mammalian Embryogenesis** *Dev. Cell* **35**:366–382
9. Brons I.G.M. *et al.* (2007) **Derivation of pluripotent epiblast stem cells from mammalian embryos** *Nature* **448**:191–195
10. Tesar P.J., Chenoweth J.G., Brook F.A., Davies T.J., Evans E.P., Mack D.L., Gardner R.L., McKay R.D.G (2007) **New cell lines from mouse epiblast share defining features with human embryonic stem cells** *Nature* **448**:196–199
11. Weinberger L., Ayyash M., Novershtern N., Hanna J.H (2016) **Dynamic stem cell states: naive to primed pluripotency in rodents and humans** *Nat. Rev. Mol. Cell Biol* **17**:155–169
12. Guo G., Yang J., Nichols J., Hall J.S., Eyres I., Mansfield W., Smith A (2009) **Klf4 reverts developmentally programmed restriction of ground state pluripotency** *Development* **136**:1063–1069
13. Takahashi S., Kobayashi S., Hiratani I (2018) **Epigenetic differences between naïve and primed pluripotent stem cells** *Cell. Mol. Life Sci* **75**:1191–1203
14. Bao S., Tang F., Li X., Hayashi K., Gillich A., Lao K., Surani M.A (2009) **Epigenetic reversion of post-implantation epiblast to pluripotent embryonic stem cells** *Nature* **461**:1292–1295
15. Habibi E. *et al.* (2013) **Whole-genome bisulfite sequencing of two distinct interconvertible DNA methylomes of mouse embryonic stem cells** *Cell Stem Cell* **13**:360–369

16. Leitch H.G. *et al.* (2013) **Naive pluripotency is associated with global DNA hypomethylation** *Nat. Struct. Mol. Biol* **20**:311–316
17. Singer Z.S., Yong J., Tischler J., Hackett J.A., Altinok A., Surani M.A., Cai L., Elowitz M.B (2014) **Dynamic heterogeneity and DNA methylation in embryonic stem cells** *Mol. Cell* **55**:319–331
18. Factor D.C., Corradin O., Zentner G.E., Saiakhova A., Song L., Chenoweth J.G., McKay R.D., Crawford G.E., Scacheri P.C., Tesar P.J (2014) **Epigenomic comparison reveals activation of “seed” enhancers during transition from naive to primed pluripotency** *Cell Stem Cell* **14**:854–863
19. Buecker C., Srinivasan R., Wu Z., Calo E., Acampora D., Faial T., Simeone A., Tan M., Swigut T., Wysocka J (2014) **Reorganization of enhancer patterns in transition from naive to primed pluripotency** *Cell Stem Cell* **14**:838–853
20. Gerondakis S., Grumont R., Gugasyan R., Wong L., Isomura I., Ho W., Banerjee A (2006) **Unravelling the complexities of the NF-kappaB signalling pathway using mouse knockout and transgenic models** *Oncogene* **25**:6781–6799
21. Kaltschmidt C., Greiner J.F.W., Kaltschmidt B (2021) **The Transcription Factor NF-κB in Stem Cells and Development** *Cells* **10** <https://doi.org/10.3390/cells10082042>
22. Espín-Palazón R., Traver D (2016) **The NF-κB family: Key players during embryonic development and HSC emergence** *Exp. Hematol* **44**:519–527
23. Li S. *et al.* (2024) **ATG5 attenuates inflammatory signaling in mouse embryonic stem cells to control differentiation** *Dev. Cell* <https://doi.org/10.1016/j.devcel.2024.01.026>
24. Torres J., Watt F.M (2008) **Nanog maintains pluripotency of mouse embryonic stem cells by inhibiting NFκappaB and cooperating with Stat3** *Nat. Cell Biol* **10**:194–201
25. Dutta D., Ray S., Home P., Larson M., Wolfe M.W., Paul S (2011) **Self-renewal versus lineage commitment of embryonic stem cells: protein kinase C signaling shifts the balance** *Stem Cells* **29**:618–628
26. Zhang Q., Lenardo M.J., Baltimore D (2017) **30 Years of NF-κB: A Blossoming of Relevance to Human Pathobiology** *Cell* **168**:37–57
27. Mulero M.C. *et al.* (2013) **Chromatin-bound IκBα regulates a subset of polycomb target genes in differentiation and cancer** *Cancer Cell* **24**:151–166
28. Marruecos L. *et al.* (2020) **IκBα deficiency imposes a fetal phenotype to intestinal stem cells** *EMBO Rep* **21**
29. Marruecos L. *et al.* (2021) **Dynamic chromatin association of IκBα is regulated by acetylation and cleavage of histone H4** *EMBO Rep* **22**
30. Thambyrajah R. *et al.* (2024) **IκBα controls dormancy in hematopoietic stem cells via retinoic acid during embryonic development** *Nat. Commun* **15**
31. Aguilera C., Hoya-Arias R., Haegeman G., Espinosa L., Bigas A (2004) **Recruitment of IκBα to the hes1 promoter is associated with transcriptional repression** *Proceedings of the National Academy of Sciences* **101**:16537–16542

32. Alvarez-Villanueva D., Galan L., Bertran J., Floor M (2023) **Separation-of-function mutants reveal the NF- κ B-independent involvement of I κ B α in the regulation of stem cell and oncogenic programs** *bioRxiv*
33. Atlasi Y., Jafarnejad S.M., Gkogkas C.G., Vermeulen M., Sonenberg N., Stunnenberg H.G (2020) **The translational landscape of ground state pluripotency** *Nat. Commun* **11**
34. Tian T.V. *et al.* (2019) **Whsc1 links pluripotency exit with mesendoderm specification** *Nat. Cell Biol* **21**:824–834
35. Ghimire S. *et al.* (2018) **Comparative analysis of naive, primed and ground state pluripotency in mouse embryonic stem cells originating from the same genetic background** *Sci. Rep* **8**
36. Zhou W. *et al.* (2022) **DNA methylation dynamics and dysregulation delineated by high-throughput profiling in the mouse** *Cell Genom* **2** <https://doi.org/10.1016/j.xgen.2022.100144>
37. Choi J. *et al.* (2017) **Prolonged Mek1/2 suppression impairs the developmental potential of embryonic stem cells** *Nature* **548**:219–223
38. Di Stefano B. *et al.* (2019) **The RNA Helicase DDX6 Controls Cellular Plasticity by Modulating P-Body Homeostasis** *Cell Stem Cell* **25**:622–638
39. Brena D. *et al.* (2020) **Ancestral function of Inhibitors-of-kappaB regulates Caenorhabditis elegans development** *Sci. Rep* **10**
40. Hayden M.S., Ghosh S (2008) **Shared principles in NF-kappaB signaling** *Cell* **132**:344–362
41. Basak S. *et al.* (2007) **A fourth IkappaB protein within the NF-kappaB signaling module** *Cell* **128**:369–381
42. Thambyrajah R. *et al.* (2022) **I κ B α controls dormancy induction in Hematopoietic stem cell development via retinoic acid** *bioRxiv* <https://doi.org/10.1101/2022.11.17.516971>
43. Álvarez-Villanueva D. *et al.* (2023) **Separation-of-function mutants reveal the NF- κ B-independent involvement of I κ B α in the regulation of stem cell and oncogenic programs** *bioRxiv* <https://doi.org/10.1101/2023.06.21.545928>
44. Guo Y.-L (2019) **The underdeveloped innate immunity in embryonic stem cells: The molecular basis and biological perspectives from early embryogenesis** *Am. J. Reprod. Immunol* **81**
45. Pantier R., Tatar T., Colby D., Chambers I (2019) **Endogenous epitope-tagging of Tet1, Tet2 and Tet3 identifies TET2 as a naïve pluripotency marker** *Life Sci Alliance* **2** <https://doi.org/10.26508/lsa.201900516>
46. Sroczynska P., Lancrin C., Pearson S., Kouskoff V., Lacaud G (2009) **In vitro differentiation of mouse embryonic stem cells as a model of early hematopoietic development** *Methods Mol. Biol* **538**:317–334
47. Chen Q., Luo W., Veach R.A., Hickman A.B., Wilson M.H., Dyda F (2020) **Structural basis of seamless excision and specific targeting by piggyBac transposase** *Nat. Commun* **11**

48. Schneider C.A., Rasband W.S., Eliceiri K.W (2012) **NIH Image to ImageJ: 25 years of image analysis** *Nat. Methods* **9**:671–675
49. Ewels P., Afyounian E., Schuster-Boeckler B.F.K (2021) **TrimGalore: v0. 6.7-DOI via Zenodo** Zenodo <https://doi.org/10.5281/zenodo.5127899.2>
50. Langmead B., Salzberg S.L (2012) **Fast gapped-read alignment with Bowtie 2** *Nat. Methods* **9**:357–359
51. Danecek P. *et al.* (2021) **Twelve years of SAMtools and BCFtools** *Gigascience* **10** <https://doi.org/10.1093/gigascience/giab008>
52. Landt S.G. *et al.* (2012) **ChIP-seq guidelines and practices of the ENCODE and modENCODE consortia** *Genome Res* **22**:1813–1831
53. Ramírez F., Ryan D.P., Grüning B., Bhardwaj V., Kilpert F., Richter A.S., Heyne S., Dündar F., Manke T (2016) **deepTools2: a next generation web server for deep-sequencing data analysis** *Nucleic Acids Res* **44**:W160–W165
54. Stovner E.B., Sætrom P (2019) **epic2 efficiently finds diffuse domains in ChIP-seq data** *Bioinformatics* **35**:4392–4393
55. Zhang Y. *et al.* (2008) **Model-based analysis of ChIP-Seq (MACS)** *Genome Biol* **9**
56. Stark R., Brown G. (2011) **DiffBind: differential binding analysis of ChIP-Seq peak data R package version 100**
57. Gu Z., Eils R., Schlesner M., Ishaque N (2018) **EnrichedHeatmap: an R/Bioconductor package for comprehensive visualization of genomic signal associations** *BMC Genomics* **19**
58. Robinson J.T., Thorvaldsdóttir H., Winckler W., Guttman M., Lander E.S., Getz G., Mesirov J.P (2011) **Integrative genomics viewer** *Nat. Biotechnol* **29**:24–26
59. Liao Y., Smyth G.K., Shi W (2014) **featureCounts: an efficient general purpose program for assigning sequence reads to genomic features** *Bioinformatics* **30**:923–930
60. Love M.I., Huber W., Anders S (2014) **Moderated estimation of fold change and dispersion for RNA-seq data with DESeq2** *Genome Biol* **15**
61. Zhu A., Ibrahim J.G., Love M.I (2019) **Heavy-tailed prior distributions for sequence count data: removing the noise and preserving large differences** *Bioinformatics* **35**:2084–2092
62. Benjamini Y., Hochberg Y (1995) **Controlling the False Discovery Rate: A Practical and Powerful Approach to Multiple Testing** *J. R. Stat. Soc. Series B Stat. Methodol* **57**:289–300
63. Garcia-Prieto C.A., Álvarez-Errico D., Musulen E., Bueno-Costa A., Vasquez B.N., Vaquero A., Esteller M. (2022) **Validation of a DNA methylation microarray for 285,000 CpG sites in the mouse genome** *Epigenetics* **17**:1677–1685
64. Ashburner M. *et al.* (2000) **Gene ontology: tool for the unification of biology. The Gene Ontology Consortium** *Nat. Genet* **25**:25–29
65. Kanehisa M., Goto S (2000) **KEGG: kyoto encyclopedia of genes and genomes** *Nucleic Acids Res* **28**:27–30

66. Martens M. *et al.* (2021) **WikiPathways: connecting communities** *Nucleic Acids Res* **49**:D613–D621
67. Hu S. *et al.* (2022) **Transcription factor antagonism regulates heterogeneity in embryonic stem cell states** *Mol. Cell* **82**:4410–4427
68. Korotkevich G., Sukhov V., Budin N., Shpak B., Artyomov M.N., Sergushichev A (2021) **Fast gene set enrichment analysis** *bioRxiv* **60012** <https://doi.org/10.1101/060012>
69. Zhou W., Triche T.J., Laird P.W., Shen H (2018) **SeSAME: reducing artifactual detection of DNA methylation by Infinium BeadChips in genomic deletions** *Nucleic Acids Res* **46**
70. Hänzelmann S., Castelo R., Guinney J (2013) **GSVA: gene set variation analysis for microarray and RNA-seq data** *BMC Bioinformatics* **14**

Author information

Luis G Palma^δ

Program in Cancer Research. Hospital del Mar Research Institute, Barcelona, Spain, Josep Carreras Leukemia Research Institute, Barcelona, Spain, Centro de Investigación Biomédica en Red Cancer (CIBERONC), Madrid, Spain
ORCID iD: [0000-0001-5170-0507](https://orcid.org/0000-0001-5170-0507)

^δThese authors contributed equally

Daniel Álvarez-Villanueva^δ

Program in Cancer Research. Hospital del Mar Research Institute, Barcelona, Spain, Institut Investigació Biomèdica de Bellvitge (IDIBELL), L'Hospitalet de Llobregat, Barcelona, Spain

^δThese authors contributed equally

María Maqueda

Program in Cancer Research. Hospital del Mar Research Institute, Barcelona, Spain, Josep Carreras Leukemia Research Institute, Barcelona, Spain, Centro de Investigación Biomédica en Red Cancer (CIBERONC), Madrid, Spain

Mercedes Barrero

Centre for Genomic Regulation (CRG), The Barcelona Institute of Science and Technology, Barcelona, Spain

Arnau Iglesias

Program in Cancer Research. Hospital del Mar Research Institute, Barcelona, Spain, Josep Carreras Leukemia Research Institute, Barcelona, Spain, Centro de Investigación Biomédica en Red Cancer (CIBERONC), Madrid, Spain

Joan Bertran

Faculty of Sciences, Technology and Engineering, Universitat de Vic - Universitat Central de Catalunya, Vic, Spain

Damiana Álvarez-Errico

Josep Carreras Leukemia Research Institute, Barcelona, Spain

Carlos A García-Prieto

Josep Carreras Leukemia Research Institute, Barcelona, Spain

Cecilia Ballaré

Centre for Genomic Regulation (CRG), The Barcelona Institute of Science and Technology, Barcelona, Spain

Virginia Rodriguez-Cortez

Josep Carreras Leukemia Research Institute, Barcelona, Spain

Clara Bueno

Josep Carreras Leukemia Research Institute, Barcelona, Spain

August Vidal

Institut Investigació Biomèdica de Bellvitge (IDIBELL), L'Hospitalet de Llobregat, Barcelona, Spain

Alberto Villanueva

Catalan Institute of Oncology (ICO/IDIBELL), L'Hospitalet de Llobregat, Barcelona, Spain

Pablo Menéndez

Josep Carreras Leukemia Research Institute, Barcelona, Spain, Centro de Investigación Biomédica en Red Cancer (CIBERONC), Madrid, Spain, Spanish Network for Advanced Therapies (RICORS-TERAV). Carlos III Health Institute (ISCIII), Madrid, Spain, Department of Biomedicine. University of Barcelona, Barcelona, Spain, Institutio Catalana de Recerca i Estudis Avançats (ICREA), Barcelona, Spain

Gregoire Stik

Josep Carreras Leukemia Research Institute, Barcelona, Spain

Luciano Di Croce

Centre for Genomic Regulation (CRG), The Barcelona Institute of Science and Technology, Barcelona, Spain, Institutio Catalana de Recerca i Estudis Avançats (ICREA), Barcelona, Spain, Universitat Pompeu Fabra, Barcelona, Spain
ORCID iD: [0000-0003-3488-6228](https://orcid.org/0000-0003-3488-6228)

Bernhard Payer

Centre for Genomic Regulation (CRG), The Barcelona Institute of Science and Technology, Barcelona, Spain, Universitat Pompeu Fabra, Barcelona, Spain
ORCID iD: [0000-0002-4694-2082](https://orcid.org/0000-0002-4694-2082)

Manel Esteller

Josep Carreras Leukemia Research Institute, Barcelona, Spain, Centro de Investigación Biomédica en Red Cancer (CIBERONC), Madrid, Spain, Institutio Catalana de Recerca i Estudis Avançats (ICREA), Barcelona, Spain, Physiological Sciences Department, School of Medicine and Health Sciences, University of Barcelona (UB), Barcelona, Spain
ORCID iD: [0000-0003-4490-6093](https://orcid.org/0000-0003-4490-6093)

Lluís Espinosa

Program in Cancer Research. Hospital del Mar Research Institute, Barcelona, Spain, Centro de Investigación Biomédica en Red Cancer (CIBERONC), Madrid, Spain
ORCID iD: [0000-0002-2897-4099](https://orcid.org/0000-0002-2897-4099)

For correspondence: lespinosa@researchmar.net

Anna Bigas

Program in Cancer Research. Hospital del Mar Research Institute, Barcelona, Spain, Josep Carreras Leukemia Research Institute, Barcelona, Spain, Centro de Investigación Biomédica en Red Cancer (CIBERONC), Madrid, Spain
ORCID iD: [0000-0003-4801-6899](https://orcid.org/0000-0003-4801-6899)

For correspondence: abigas@researchmar.net

Editors

Reviewing Editor

Owen Tamplin

University of Wisconsin-Madison, Madison, United States of America

Senior Editor

Silke Hauf

Virginia Tech, Blacksburg, United States of America

Reviewer #1 (Public review):

Summary:

This study probes the role of the NF- κ B inhibitor I κ Ba in the regulation of pluripotency in mouse embryonic stem cells (mESCs). It follows from previous work that identified a chromatin-specific role for I κ Ba in the regulation of tissue stem cell differentiation. The work presented here shows that a fraction of I κ Ba specifically associates with chromatin in pluripotent stem cells. Using three Nfkb1a-knockout lines, the authors show that I κ Ba ablation impairs the exit from pluripotency, with embryonic bodies (an in vitro model of mESC multi-lineage differentiation) still expressing high levels of pluripotency markers after sustained exposure to differentiation signals. The maintenance of aberrant pluripotency gene expression under differentiation conditions is accompanied by pluripotency-associated epigenetic profiles of DNA methylation and histone marks. Using elegant separation of function mutants identified in a separate study, the authors generate versions of I κ Ba that are either impaired in histone/chromatin binding or NF- κ B binding. They show that the provision of the WT I κ Ba, or the NF- κ B-binding mutant can rescue the changes in gene expression driven by loss of I κ Ba, but the chromatin-binding mutant can not. Thus the study identifies a chromatin-specific, NF- κ B-independent role of I κ Ba as a regulator of exit from pluripotency.

Strengths:

The strengths of the manuscript lie in: (a) the use of several orthogonal assays to support the conclusions on the effects of exit from pluripotency; (b) the use of three independent clonal Nfkb1a-KO mESC lines (lacking I κ Ba), which increase confidence in the conclusions; and (c) the use of separation of function mutants to determine the relative contributions of the chromatin-associated and NF- κ B-associated I κ Ba, which would otherwise be very difficult to unpick.

Weaknesses:

In this reviewer's view, the term "differentiation" is used inappropriately in this manuscript. The data showing aberrant expression of pluripotency markers during embryoid body formation are supported by several lines of evidence and are convincing. However, the authors call the phenotype of Nfkb1a-KO cells a "differentiation impairment" while the data on differentiation markers are not shown (beyond the fact that H3K4me1, marking poised enhancers, is reduced in genes underlying GO processes associated with differentiation and organ development). Data on differentiation marker expression from the transcriptomic and embryoid body immunofluorescent experiments, for example, should be at hand without the need to conduct many more experiments and would help to support the conclusions of the study or make them more specific. The lack of probing the differentiation versus pluripotency genes may be a missed opportunity in gaining in-depth understanding of the phenotype associated with loss of the chromatin-associated function of IκBα.

<https://doi.org/10.7554/eLife.102784.1.sa2>

Reviewer #2 (Public review):**Summary:**

This manuscript investigates the role of IκBα in regulating mouse embryonic stem cell (ESC) pluripotency and differentiation. The authors demonstrate that IκBα knockout impairs the exit from the naïve pluripotent state during embryoid body differentiation. Through mechanistic studies using various mutants, they show that IκBα regulates ESC differentiation through chromatin-related functions, independent of the canonical NF-κB pathway.

Strengths:

The authors nicely investigate the role of IκBα in pluripotency exit, using embryoid body formation and complementing the phenotypic analysis with a number of genome-wide approaches, including transcriptomic, histone marks deposition, and DNA methylation analyses. Moreover, they generate a first-of-its-kind mutant set that allows them to uncouple IκBα's function in chromatin regulation versus its NF-κB-related functions. This work contributes to our understanding of cellular plasticity and development, potentially interesting a broad audience including developmental biologists, chromatin biology researchers, and cell signaling experts.

Weaknesses:

- The study's main limitation is the lack of crucial controls using bona fide naïve cells across key experiments, including DNA methylation analysis, gene expression profiling in embryoid bodies, and histone mark deposition. This omission makes it difficult to evaluate whether the observed changes in IκBα-KO cells truly reflect naïve pluripotency characteristics.
- Several conclusions in the manuscript require a more measured interpretation. The authors should revise their statements regarding the strength of the pluripotency exit block, the extent of hypomethylation, and the global nature of chromatin changes.
- From a methodological perspective, the manuscript would benefit from additional orthogonal approaches to strengthen the knockout findings, which may be influenced by clonal expansion of ES cells.

Overall, this study makes an important contribution to the field. However, the concerns raised regarding controls, data interpretation, and methodology should be addressed to strengthen the manuscript and support the authors' conclusions.

<https://doi.org/10.7554/eLife.102784.1.sa1>

Author response:

eLife Assessment

This important study reveals a role for IκBα in the regulation of embryonic stem cell pluripotency. The solid data in mouse embryonic stem cells include separation of function mutations in IκBα to dissect its non-canonical role as a chromatin regulator and its canonical function as NF-κB inhibitor. The conclusions could be strengthened by including better markers of differentiation status and additional controls or orthogonal approaches.

We are thankful to the two reviewers and editors for their kind feedback and for highlighting the impact of NF-κB-independent IκBα function in stabilizing naïve pluripotency.

In order to address reviewer's comments, we will perform further analysis of differentiation trajectories, as well as a deeper comparison of the epigenetic features in our IκBα-KO mESCs with the Serum/LIF and 2i/LIF conditions. Moreover, we recognize that some sentences need to be modified to soften our conclusions in terms of effects on block in the naïve state or the global epigenetic effects, as the reviewers pointed out.

Public Reviews:

Reviewer #1 (Public review):

Summary:

This study probes the role of the NF-κB inhibitor IκBα in the regulation of pluripotency in mouse embryonic stem cells (mESCs). It follows from previous work that identified a chromatin-specific role for IκBα in the regulation of tissue stem cell differentiation. The work presented here shows that a fraction of IκBα specifically associates with chromatin in pluripotent stem cells. Using three Nfkb1a-knockout lines, the authors show that IκBα ablation impairs the exit from pluripotency, with embryonic bodies (an in vitro model of mESC multi-lineage differentiation) still expressing high levels of pluripotency markers after sustained exposure to differentiation signals. The maintenance of aberrant pluripotency gene expression under differentiation conditions is accompanied by pluripotency-associated epigenetic profiles of DNA methylation and histone marks. Using elegant separation of function mutants identified in a separate study, the authors generate versions of IκBα that are either impaired in histone/chromatin binding or NF-κB binding. They show that the provision of the WT IκBα, or the NF-κB-binding mutant can rescue the changes in gene expression driven by loss of IκBα, but the chromatin-binding mutant can not. Thus the study identifies a chromatin-specific, NF-κB-independent role of IκBα as a regulator of exit from pluripotency.

Strengths:

The strengths of the manuscript lie in: (a) the use of several orthogonal assays to support the conclusions on the effects of exit from pluripotency; (b) the use of three independent clonal Nfkb1a-KO mESC lines (lacking IκBα), which increase confidence in the conclusions; and (c) the use of separation of function mutants to determine the relative contributions of the chromatin-associated and NF-κB-associated IκBα, which would otherwise be very difficult to unpick.

Weaknesses:

In this reviewer's view, the term "differentiation" is used inappropriately in this manuscript. The data showing aberrant expression of pluripotency markers during

embryoid body formation are supported by several lines of evidence and are convincing. However, the authors call the phenotype of Nfkb1a-KO cells a "differentiation impairment" while the data on differentiation markers are not shown (beyond the fact that H3K4me1, marking poised enhancers, is reduced in genes underlying GO processes associated with differentiation and organ development). Data on differentiation marker expression from the transcriptomic and embryoid body immunofluorescent experiments, for example, should be at hand without the need to conduct many more experiments and would help to support the conclusions of the study or make them more specific. The lack of probing the differentiation versus pluripotency genes may be a missed opportunity in gaining in-depth understanding of the phenotype associated with loss of the chromatin-associated function of IκBα.

Specific answer to weaknesses for Reviewer 1:

We have data showing the lack of expression of specific differentiation markers that we will add to the manuscript. Moreover, we will also globally analyse differentiation markers in our transcriptomic data to have a more accurate description of the phenotype.

Reviewer #2 (Public review):

Summary:

This manuscript investigates the role of IκBα in regulating mouse embryonic stem cell (ESC) pluripotency and differentiation. The authors demonstrate that IκBα knockout impairs the exit from the naïve pluripotent state during embryoid body differentiation. Through mechanistic studies using various mutants, they show that IκBα regulates ESC differentiation through chromatin-related functions, independent of the canonical NF-κB pathway.

Strengths:

The authors nicely investigate the role of IκBα in pluripotency exit, using embryoid body formation and complementing the phenotypic analysis with a number of genome-wide approaches, including transcriptomic, histone marks deposition, and DNA methylation analyses. Moreover, they generate a first-of-its-kind mutant set that allows them to uncouple IκBα's function in chromatin regulation versus its NF-κB-related functions. This work contributes to our understanding of cellular plasticity and development, potentially interesting a broad audience including developmental biologists, chromatin biology researchers, and cell signaling experts.

Weaknesses:

- The study's main limitation is the lack of crucial controls using bona fide naïve cells across key experiments, including DNA methylation analysis, gene expression profiling in embryoid bodies, and histone mark deposition. This omission makes it difficult to evaluate whether the observed changes in IκBα-KO cells truly reflect naïve pluripotency characteristics.*
- Several conclusions in the manuscript require a more measured interpretation. The authors should revise their statements regarding the strength of the pluripotency exit block, the extent of hypomethylation, and the global nature of chromatin changes.*
- From a methodological perspective, the manuscript would benefit from additional orthogonal approaches to strengthen the knockout findings, which may be influenced by clonal expansion of ES cells.*

Overall, this study makes an important contribution to the field. However, the concerns raised regarding controls, data interpretation, and methodology should be addressed to strengthen the manuscript and support the authors' conclusions.

Specific answer to weaknesses for Reviewer 2:

- As the reviewer pointed out, we have not performed all the analysis by comparing with cells in 2i LIF since our initial study was focused on Serum LIF and differentiation. However, it was the transcriptome analysis in Serum LIF which showed that KO cells resembled naïve ES cells in 2i LIF by GSEA. We have repeated key experiments with all conditions (Figure 1B, 1D, Figure 3C and 3), but we do not think that repeating all 'omics' experiments with 2i LIF conditions will add important information. Nevertheless, we will analyze different chromatin data (DNA methylation and different histone post-translational modifications) from previously published works in 2i/LIF and Serum/LIF and compare them with our I κ B α -WT and I κ B α -KO mESCs to better confirm the stabilization of the ground state pluripotency in I κ B α -KO mESCs under Serum/LIF conditions.

- We agree about reducing the strength of the pluripotency exit block, extend of hypomethylation and the global nature of chromatin changes. There are many changes in the chromatin that we are trying to better characterize by HiC in ongoing studies that are out of the scope of this manuscript.

We have performed studies in 3 different I κ B α KO and WT clones. In addition, the reconstitution studies with I κ B α separation-of-function (SOF) mutants with differential effect after expressing the NF κ B binding form (I κ B α DChrom) or the chromatin binding form (I κ B α DNF κ B) also support the robustness of this phenotype.

<https://doi.org/10.7554/eLife.102784.1.sa0>